Validation of the TRMM PR rain retrieval algorithm from airborne and ground-based radar data

Paul Amayenc

with contributions from

Franck Ferreira, Erwan Le Bouar, Stéphane Oury, and Jacques Testud

CETP, Vélizy, France

Foreword

The present report reflects the scientific content of a presentation given at ECMWF/ EuroTRMM Workshop on «Assimilation of Clouds and Precipitation», held at ECMWF on 6-9 November 2000. The underlying work was accomplished in the framework of Euro TRMM program, sponsored by European Community and ESA. More precisely, it covers the task 4100, and part of the task 3100, as labeled in the genuine work packages description. Objective of task 4100 was to study the performances of the rain profiling algorithm of the TRMM precipitation radar. Part of task 3100 involved here aimed at testing rain products derived from the TRMM precipitation radar by means of «reference» products derived from the exploitation of ground-based or airborne radar measurements, gathered in coincidence with TRMM observations in the same rainy systems. Besides, a large part of the report is reprentative of results obtained by F. Ferreira (CETP) in the framework of a Doctotate Thesis.

1. Objectives and overview of the study

The Precipitation Radar (PR) of the Tropical Rainfall measuring Mission (TRMM) is an unprecedented tool for observing precipitation from space, in addition to the VIS/IR radiometer and the TRMM microwave imager (TMI) on board the platform. The operating frequency (13.8 GHz), and the cross-range resolution (about 4.2 km at nadir) of the radar requires that the two-way path-integrated attenuation (PIA), and non uniform beam filling (NUBF) effects (*Amayenc et al.*, 1993), be corrected to reduce bias in rain estimation. These are the main two challenges that the PR standard rain-profiling algorithm, labeled by 2A-25 in the «TRMM» nomenclature, has to face (*Iguchi et al.*, 2000). Also, rain rate estimates depend on the selected relations between the integrated rainfall parameters, and the way they are adjusted in the algorithm.

The standard TRMM algorithms, including the 2A-25, were revised several times, and hopefully improved since the TRMM launching (at the end of November 1997). The version-4 2A-25 was changed to the presently-operating version 5 by mid fall of 1999. Accordingly, TRMM data acquired since the launching were reprocessed at NASA/TSDIS between November 1999 and April 2000. Tests performed with the version-4 2A-25 were reported to underestimate the rain rate (R) relative to other ground-based or space-based estimates such as monthly zonal averages derived from TMI or TMI/PR combination (*Iguchi et al.*, 2000). Version-5 algorithm aims at alleviating these kinds of discrepancies. New upgraded versions of the algorithm are planned to be regularly developed in future. Analyzing possible deficiencies of the algorithm, appreciating improvements brought by any new version, and help suggesting new development, are sound works for TRMM experimenters.

The present work was performed in such a context during the Euro TRMM study. The objective was to analyze the functioning of the TRMM PR "standard" algorithm 2A-25, study possible improvements in rain rate estimates, then test and possibly validate these improvements. It was also expected to derive useful quantities like rain rate and liquid water content estimates, along with rain-dimensioning parameter(s) like scaling-parameter of the drop size distribution (DSD), which could be further used as ingredients of synergetic algorithms combining PR and microwave radiometer (TMI) data, developed elsewhere in the Euro TRMM study. This was of prime importance to expect generating "good" rain products for assimilation in ECMWF model, and/or testing convection schemes in NWP models, as done in other Euro TRMM tasks.

The date at which version-5 TRMM data became progressively available (end of 1999 for current observations, and April 2000 for reprocessed data) occurred well after the Euro TRMM study kick-off (Feb. 1998, for a 3-year period). This fact, along with the necessity to exchange results with other partners without jeopardizing the self consistency and planned time schedule of the Euro TRMM study, prevented us to focuse all our efforts on the analysis of the updated version-5 PR products. Therefore, a basic part of the study deals with version-4 PR products that are now obsolete. However, this is not a strong drawback for the following reasons: i) version-4 products are still widely used (and will likely be used for a time in future) by many searchers owing to the several-month time delay required for editorial process of formal publications; ii) analytical aspects developed in the study remain valid in the framework of version-5; iii) some version-5 PR products could be included in our analysis. Such considerations illustrate the advantage/drawback balance inherent to TRMM data handling: the fast regular upgrading of the algorithm versions is beneficial for science, but somewhat in conflict with the time required for analyzing and validating new products.

In the present work, possible improvements of the version-4 2A-25, obtainable from different adjustments of the prescribed initial rain relations, were explored using two alternatives to the standard rain rate. Also, improvements in R-estimate brought by the standard version-5 with respect to the standard version-4 2A-25 algorithm, were analyzed. With the version 4, the first alternative rain rate (R_{N0}) exploits the concept of normalized rain drop-size distribution (DSD) to scale the rain relations via a relevant parameter, N_0^* (*Dou et al.*, 1999; *Testud et al.*, 2000). The second one (R_{kR}) exploits the relation between R and the attenuation coefficient (k), instead of Z as in the standard estimate ($R_{std\text{-}V4}$). This allows us to study effects of various error sources and determine limits on accuracy in rain retrieval expected from a single-frequency radar such as TRMM PR. A preliminary study of such computable R-estimates using data of the airborne TRMM PR simulator, ARMAR (*Durden et al.*, 1994) in TOGA-COARE (*Webster and Lukas*, 1992), was presented in *Marécal et al.* (1997), and *Tani and Amayenc* (1998). The computational parameters can be easily obtained from the output file of the standard version-4 2A-25 without changing the physical concepts used in the algorithm. The alternative approaches could be also used in the framework of the version-5 2A-25, but they would imply a full reprocessing of the algorithm after implementing additional specific coding, which has not been attempted yet.

In the framework of version 4, the reliability of the alternative rain estimates compared with the standard one was tested from a TRMM PR data set. The same PR data set was also used to compare standard version-5 ($R_{std\text{-}V5}$) and standard version-4 ($R_{std\text{-}V4}$) results. Finally, the reliability of the various PR-derived estimates was tested by using airborne or ground based (GB) radar data to generate rain-related reference products, and compare them with the PR-derived products for coincident observations in the same rainy systems. A large part of the study reflects the content of *Ferreira et al.*, 2000.

The presentation of the work is organized as follows. The basic physical concepts used in the standard 2A-25 algorithm, are outlined in section 2. Adjustment of rain relations, alternative R-estimates, and a sensitivity study to various error sources are presented in section 3; this section also includes an approach to generate liquid water content (W) estimates usable in synergetic radar/radiometer algorithm(s). Then, detailed results on rain estimates from PR data gathered in hurricane Bonnie during CAMEX-3 (1998), along with mean features emerging from a PR data set over ocean and land, are discussed in section 4. A point-to-point comparison of PR-derived 3-D Z- and R-fields to those gathered from airborne X-band dual-beam radar data in hurricanes Bonnie (26 Aug. 1998), and Brett (21 Aug. 1999), over Mexico Gulf, for good cases of TRMM overpass, is presented in section 5. A similar approach, but using reference data from the C-band polarimetric radar located at the TRMM ground validation (GV) site of Darwin (Australia), is presented in section 6. Application of a new algorithm (*Testud et al.*, 2000b) to exploit polarimetric radar data gives additional access to the scaling parameter (N_0^*) of the rain relations, which is also derived from the PR and needs to be validated. Conclusions are given in section 7. Details of some mathematical developments are given in appendix.

2. Outlook of the standard 2A-25 rain profiling algorithm

The flowch art of the standard TRMM PR algorithms is shown in Fig. 1. The 2A-25 algorithm functioning is detailed in *Iguchi et al* (2000). The basic concepts of the algorithm, used in version 4 are described below, with some emphasis on aspects that are more specifically addressed further in the present study. Then, the main differences between versions 4 and 5 of the algorithm are mentioned.

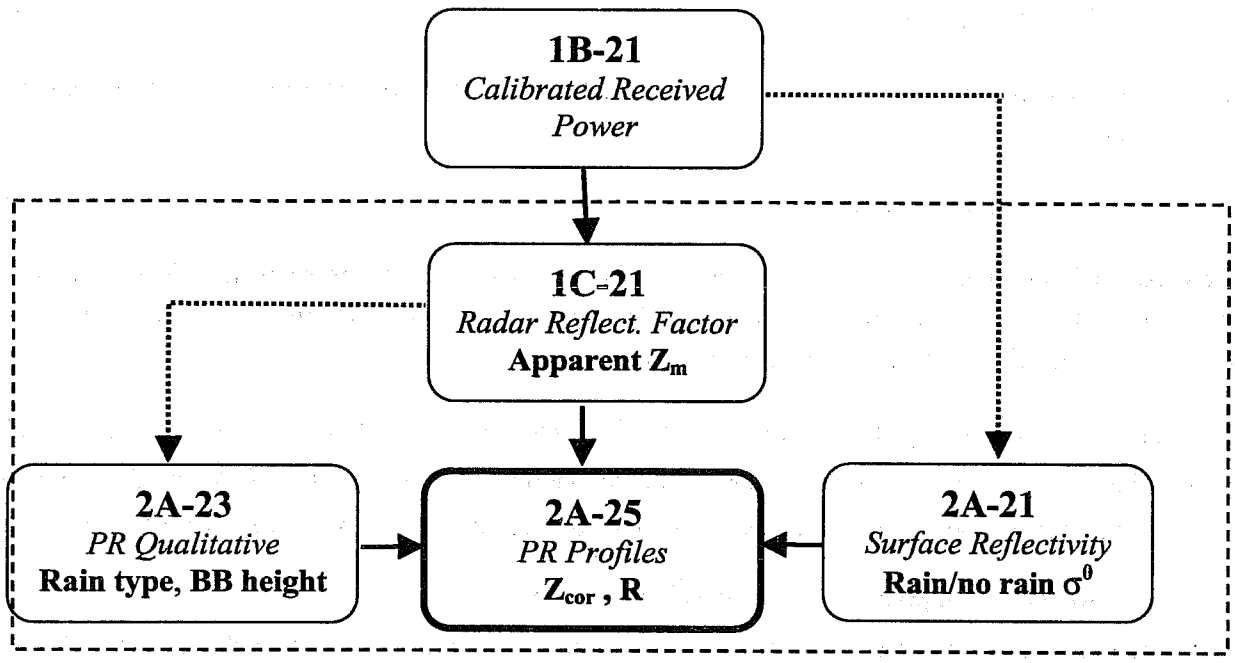

Fig. 1: Flowchart of the TRMM PR "standard" algorithms (Levels 1 and 2) with their inter-connections. BB stands for bright-band (melting ice particles). σ° is the surface backsactter coefficient. The Euro TRMM study makes use of algorithms inside the dotted box.

2.1 Basic physical concepts used in version-4

The 2A-25 algorithm adjusts, for every path, the coefficient α in the chosen initial relation

$$k = \alpha Z^{\beta} \tag{1}$$

by means of a range-free correction factor $\varepsilon=\delta\alpha$ that is further used to compute the two-way PIA factor to any range r. In practice, this factor has the hybrid form

$$\varepsilon_1 = 1 - W + W\varepsilon_0 \tag{2}$$

where w is a normalized weight ($0 \le w \le 1$), and ε_0 is the correction factor based on the surface reference (SR) technique (*Meneghini et al.*, 1983; *Meneghini and Nakamura*, 1990). The weight w is a function of the total PIA factor to the surface (at range r_s), $A_{HB}(r_S)$, estimated from the solution of *Hitschfeld and Bordan* (1954) (HB), and the SR-based total PIA factor, $A_S(r_S)$, given respectively by:

$$A_{HB}(r_S) = [1-\gamma S(0,r_S)]^{1/\beta} \tag{3}$$

where $\gamma = 0.2\ln(10)\beta = 0.46\beta$, and

$$S(r_1, r_2) = \int_{r1}^{r2} \alpha Z_m^{\beta}(s)\,ds \tag{4}$$

and

$$A_S(r_S) = [1-\gamma\varepsilon_0 S(0,r_S)]^{1/\beta} \tag{5}$$

In (4), Z_m is the «apparent» or measured reflectivity factor. The SR-based correction factor ε_0 is computed from (5), according to

$$\varepsilon_0 = [1 - A_S^{\beta}(r_S)]\,\gamma^{-1}(0,r_S)^{-1} \tag{6}$$

where $A_S(r_S)$ is provided by the 2A-21 algorithm from surface echo measurements (*Meneghini et al.*, 2000), and $Z_m(r)$ in $S(0,r_s)$ is provided by the 1C-21 algorithm. It is assumed that Z_m is not biased by an error in the radar calibration, and $A_S(r_S)$ is error free.

The total PIA magnitude is judged from an attenuation factor index $\zeta=S(0,r_S)=1-A_{HB}^{\beta}$ derived from (3). The weighting of ε_f towards ε_0 in (2) increases with the magnitude of the HB-based PIA, and the reliability of the SR-based PIA. The resulting PIA factor, $A_f(r)$, is the hybrid of $A_{HB}(r)$ and $A_S(r)$, according to:

$$A_f^{\beta}(r) = [1-\gamma\varepsilon_f S(0,r)] = (1-w)A_{HB}^{\beta}(r) + wA_S^{\beta}(r) \tag{7}$$

The attenuation-corrected reflectivity factor profile, computed as $Z(r)=Z_m(r)/A_f(r)$, is the hybrid of the HB-based solution that does not perform α-correction ($\varepsilon=1$), and the SR-based solution with α-adjustment ($\varepsilon=\varepsilon_0$). The retrieved Z is close to the HB-based (resp. SR-based) solution for low (resp. large) PIA with $w\approx 0$ (resp. $w\approx 1$). The hybrid scheme avoids known potential divergence of the HB-based solution for high PIA, or large error in the SR-based solution for low or unreliable PIA. Most of the time, α-adjustment is hybrid with ε_f lying between 1 (HB case) and ε_0 (SR case).

Also, the algorithm performs, for each beam, a range-free correction of NUBF effects based on a statistical scheme that involves PR data for the eight beams surrounding the angle bin in question to determine the index of non uniformity (*Kozu and Iguchi*, 1999).

The *standard version-4 rain rate estimate, further referred to as* $R_{std\text{-}V4}$, is derived from the «true» Z via a prescribed initial relation,

$$R = aZ^b, \tag{8}$$

where a is corrected for NUBF effects.

Initial coefficients α, a, and b, in relations k-Z (1), or R-Z (8), are functions of height according to changes in temperature, phase, and pressure (for R-Z). They also depend on rain type (as categorized by the 2A-23 algorithm) that is determined by the horizontal and vertical storm structure model (*Iguchi et al.*, 2000). Coefficient β in k-Z is assumed range-free. In version 4, the initial coefficients for rain are modeled from ground-based distrometer data from Darwin (Australia), assuming Γ-shaped DSD with a shape parameter μ=1. For ice, or mixed phase, the initial coefficients are modeled assuming prescribed ice density, or mixing ratio. Therefore, the height profile of all initial coefficients (except β) may change from beam to beam, according to the rain type and storm model.

Ill-adapted initial rain relations may induce significant errors in the rain estimates, especially for low PIA (i.e. in stratiform light rain) since the HB-based solution does not perform an adjustment. For large PIA (i.e. in convective rain), the SR-based solution adjusts the k-Z relation. However, the initial R-Z relation is not modified. Hence, it was found useful to look for self-consistent scaling of the involved rain relations, and alternatives to the standard version-4 rain rate estimate.

2.2 Main changes from version 4 to version 5

Major changes in version 5 with respect to version 4 are:

1) Modified inputs from other algorithms dealing with the computation of σ^0 in clear air for the SR (2A-21 algorithm), the rain-type classification (2A-23 algorithm), and a correction of the radar calibration that increases Z_m by 0.52 dB (1C-21 algorithm);

2) A better identification of the range of useful signal, and noise elimination;

3) A slightly modified vertical structure of the storm model;

4) An improved calculation of the correction factor ε_p which is based on a statistically-objective, instead of arbitrarily-prescribed HB/SR weighting that takes into account the estimated errors in the HB-based and SR-based total PIA's;

5) Modifications of the initial rain relations, k-Z, and R-Z, relying on a world-wide averaged empirical, instead of the Darwin-based DSD model;

6) The use of an adjusted, instead of initial constant, R-Z relation, the coefficients of which are modified in accordance with the α-adjustment in k-Z relation, and the DSD model, after *Kozu et al.* (1999).

Points 1 to 3 are mostly «technical» improvements. Points 4 to 6 are the most important ones. Concerning point 6, the method used to adjust the rain relations, then obtain the *standard version-5 rain rate estimate, further referred to as* $R_{std\text{-}V5}$, differs from the N_0^*-scaling used in the present study with the version 4 (see section 3.1).

3. Alternative rain estimates to the version-4 2A-25 standard

In the framework of version-4, two alternatives to the standard rain rate estimate, inspired by previous works (e. g. *Tani and Amayenc*, 1998, *Durden and Haddad*, 1998, *Ferreira and Amayenc*, 1999), can be defined. The first one uses a scaling of rain relations exploiting the concept of normalized DSD. The second one uses a constant R-k relation

$$R = ek^d \tag{9}$$

instead of a constant R-Z relation (8) as in the standard. These approaches are explained below.

3.1 Principle of N_0^*-scaling and adjustment of rain relations

The concept of normalized Γ-shaped DSD (*Dou et al.*, 1999a,b) allows any two integrated rainfall parameters (X,Y) to obey

$$X = mN_0^{*(1-n)}Y^n \tag{10}$$

where m does not depend, and n weakly depends on the DSD shape parameter μ (*Ulbrich*, 1983), provided that X and Y be close to DSD moments. N_0^* is a μ-free scaling parameter which identifies with the "classical" N_0 intercept of the exponentially-shaped DSD having the same water content, and mean volume diameter, D_m, as those of the Γ-shaped DSD. Using D_m instead of the median volume diameter D_0 (as in *Dou et al.*, 1999a,b) is more convenient for practical application (*Testud et al.*, 2000a). In (10), m and n can be computed from fits to a scattering/attenuation model using experimental data. Thus, any rain relation can be scaled by N_0^*. Note that the X-Y relation becomes less sensitive to N_0^*-scaling as n approaches 1.

The afore-mentioned property was exploited to compute the reference N_0^* implied by the initial relations used in the 2A-25 algorithm, for stratiform or convective rain. The initial rain relations were compared with a set of normalized relations computed for different N_0^* using Mie calculations, horizontal polarization at 13.8 GHz, μ=1 (in accordance with the underlying DSD model in 2A-25), and temperatures ranging from 0° to 20°C. The reference N_0^* was then determined, in each case, by identifying which N_0^* yields the normalized relation best fitting (in the least square sense) to the initial relation within the [20-50] dBZ range of Z. Fig. 2 displays such a comparison for the k-Z relation at 20°C. The computed N_0^* changes by about ±20% depending on the relation (k-Z or R-Z), and temperature.

The inferred version-4 initial N_0^* for stratiform or convective rain are listed in Table 1: They agree fairly well with results obtained in TOGA-COARE, while they are about half (resp. twice) the reference value (0.8×10^6 m^{-4}) of *Marshall and Palmer* (1948). The TOGA-COARE results refer to mean values derived from airborne DSD data gathered with 2-DP PMS probes during 15 flights. The numbers given in *Dou et al.* (1999a,b) are slightly revised here owing to using D_m instead of D_0. Results for total rain are only indicative since they are computed as the mean of convective and stratiform rain cases while ignoring any weighting by the relative volume (or area) of each rain type. Inferred version-5 initial N_0^* results are also

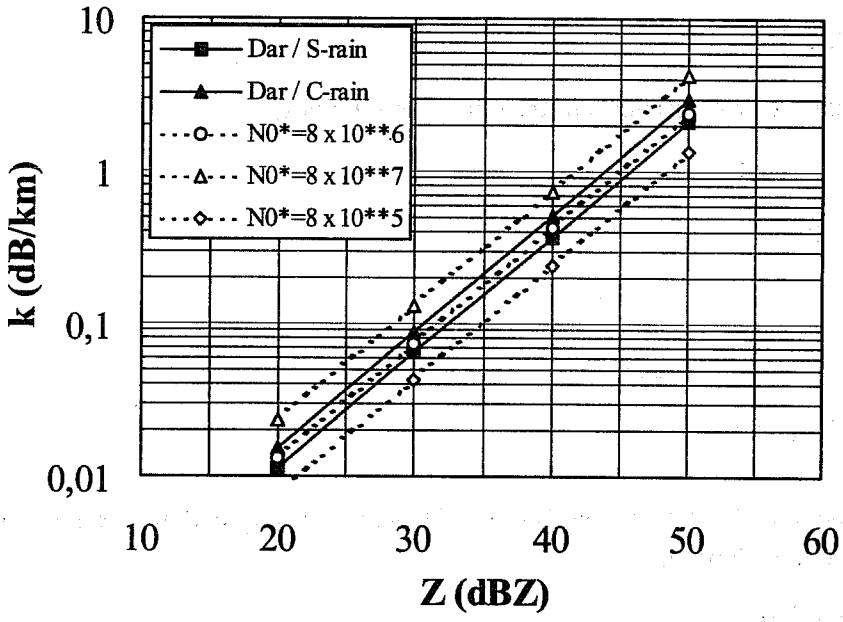

Fig. 2: k-Z rain relations at K_u-band derived from «normalized»Γ-shaped DSD (μ=1, T=20°C, Mie conditions) for different values of N_0^* (m^{-4}); and initial k-Z rain relations (T=20°C) used in the version-4 2A-25 algorithm for stratiform (S), and convective (C) rain, as inferred from Darwin data (see text).

listed in Table 1. Though based on a different DSD model (see section 2.2), they are fairly close to the version-4 results, except for S-rain.

Case	*C-rain*	S- rain	*Total rain*
2A-25 initial / Version-4	16.6	5.1	10.9
2A-25 initial / Version-5	15.7	7.4	11.6
TOGA-COARE (data set average)	14.3	3.1	8.7
Marshall-Palmer	8	8	8

Table 1: Initial N_0^* (in 10^6 m^{-4}) inferred from the 2A-25 algoritm initial relations (versions 4 and 5) compared with other reference values, for convective (C), stratiform (S), and total rain (mean of C- and S-rain).

According to (10), with k as X and Z as Y, the $\delta\alpha$-correction to α_{init} (via the correction factor ε) in the k-Z relation, may be interpreted as δN_0^*-correction to the initial $N_{0\,init}^*$. Using

$$k = \alpha_{init}\delta\alpha Z^{\beta} \tag{11}$$

with

$$\delta\alpha \equiv \delta N_0^{*(1-\beta)} = \varepsilon, \tag{12}$$

yields

$$\delta N_0^* = \varepsilon^{1/(1-\beta)} \tag{13}$$

and the «adjusted» N_0^*:

$$N_{0\,adj}^* = N_{0\,init}^* \, \delta N_0^* \tag{14}$$

Next, δN_0^* can be used to scale coefficients of the other two relations,

$$R = a_{init} \, \delta a \, Z^b, \text{ and} \tag{15a}$$

$$R = e_{init} \, \delta e \, k^d, \tag{15b}$$

according to

$$\delta a \equiv \delta N_0^{*\,(1-b)} = \varepsilon^{(1-b)/(1-\beta)}, \text{ and} \tag{16a}$$

$$\delta e \equiv \delta N_0^{*\,(1-d)} = \varepsilon^{(1-d)/(1-\beta)}. \tag{16b}$$

Self-consistency of the initial relations set (1) (8) (9), which is required to get any relation from a combination of the other two, implying

$$a = e\alpha^d \; ; \; d = b/\beta, \tag{17}$$

is maintained in N_0^*-scaled relations.

In practice, the hybrid character of α-adjustment in the 2A-25, via ε_f, leads to hybrid N_0^*-scaling discussed in section 3.3.

The above-defined N_0^*-scaling can be usefully compared with the N_0-adjustment of *Kozu et al.* (1999) used in the version-5 2A-25 (see section 2.2). In the latter method, the assumed DSD model is built from a set of rain-type dependent Z-R relations measured near ocean at various places over the world. The Z-R relation is converted into the relation between N_0 and Λ of a Γ-shaped DSD with a shape parameter μ=3. The corresponding k-Z and Z-R relations at 13.8 GHz are calculated for rain, snow at different temperatures and different mixing ratios. Initial coefficients a and b in $R=aZ^b$ are adjusted when α in $k=\alpha Z^\beta$ is adjusted, in such a way that the adjusted pair (a,b) is consistent with the pair (α,β) in $k=\alpha Z^\beta$ when they are both converted into the N_0-Λ of the DSD model. The value chosen for μ has weak impact on the derived k-Z and R-Z relations. In practice, the correction factors to a and b are expressed as quadratic functions of $\log(\varepsilon_f)$. Therefore, both N_0^*-scaling and N_0-adjustment allow self-consistent though different scaling of the rain relations. However, the two coefficients of the R-Z relations are adjusted in Kozu's approach, instead of only one in N_0^*-scaling. Besides, the adjustment is performed via numerical functions in the former case, instead of analytical approach in the latter one.

3.2 Standard and alternative rain rate estimates

The computation principle of rain estimates, taking into account potential error terms, is given below. Error in a given parameter x is still defined as a unitless multiplying factor δx, thereby providing a "corrected" value (x δx). Following *Tani and Amayenc* (1998)., the reasoning starts from the expression for the specific attenuation coefficient k(r), then comes to the expression(s) for the reflectivity factor Z(r), and finally the rain rate R(r).

A general expression for the k(r) estimate is:

$$k(r) = \alpha Z_m(r)^{\beta} \varepsilon A(r,\varepsilon)^{-\beta} \tag{18}$$

where

$$\varepsilon \equiv \delta\alpha\delta C^{-\beta} \tag{19}$$

is the product of scaling errors (assumed to be range-free) in $(\alpha Z_m{}^{\beta})$ product, C is the radar calibration constant, and $A(r,\varepsilon)$ is the PIA factor to range r, given by:

$$A(r,\varepsilon) = [1-\gamma\varepsilon S(0,r)]^{1/\beta} \tag{20}$$

The Z(r) estimate, using (19), is:

$$Z(r) \equiv Z_m(r)A(r,\varepsilon)^{-1}\delta C^{-1} = Z_m(r)A(r,\varepsilon)^{-1}\delta\alpha^{-1/\beta}\varepsilon^{1/\beta} \tag{21}$$

Then, using either (15a) or (15b), and (11), (21), (17), the "true" $R_t(r)$ estimate becomes:

$$R_t(r) = aZ_m(r)^b A(r,\varepsilon)^{-b}\delta C^{-b}\,\delta a = aZ_m(r)^b A(r,\varepsilon)^{-b}\varepsilon^d\,\delta e \tag{22}$$

The computable k-, Z-, and R-estimates depend on the way followed to evaluate $A(r,\varepsilon)$, and the various error terms. The HB-based solution assumes $\varepsilon=1$, and $\delta C=\delta\alpha=\delta a=\delta e=1$ (no-adjustment) in all estimates, and therefore may be corrupted by «uncorrected» errors. The SR-based solution identifies the «measured» correction factor ε_0 (6) with the product of error terms ε (19). Using $\varepsilon=\varepsilon_0$ in (18) and (20), yields the k-estimate:

$$k(r) = \alpha Z_m{}^{\beta}\varepsilon_0 A(r,\varepsilon_0)^{-\beta} \tag{23}$$

which does not require the correction type (δC or $\delta\alpha$) being specified, since (19) involves the product of errors, only.

For computing Z, the correction type must be specified. In C-adjustment (ignoring $\delta\alpha$, i.e. $\varepsilon_0=\delta C^{-\beta}$, $\delta\alpha=1$), (21) yields:

$$Z_C = Z_m \varepsilon_0^{1/\beta} A(r,\varepsilon_0)^{-1} \tag{24}$$

while in α-adjustment (ignoring δC, i.e. $\varepsilon_0=\delta\alpha$, $\delta C=1$), it yields:

$$Z_\alpha = Z_m\, A(r,\varepsilon_0)^{-1} = Z_C\, \varepsilon_0^{-1/\beta} \tag{25}$$

which is the standard Z-estimate for the «true» SR-case. Of course, Z_C (resp. Z_α) may be corrupted by $\delta\alpha$ (resp. δC) via the term $\delta\alpha^{-1/\beta}$ in (24) (resp. δC^{-1} in (25)). The α- and C-adjustments are basically different despite the similarities of the two adjustment process because adjusting α (or N_0^*) on a beam-to-beam basis is likely reasonable owing to the variability in the DSD, while adjusting C in such a way is not when considering the reported stability in the PR calibration (*Iguchi et al.*, 2000).

The rain rate R_C associated to Z_C is derived from (22) with $\varepsilon=\varepsilon_0=\delta C^{-\beta}$, and $\delta a=\delta e=1$, as

$$R_C = aZ_m{}^b A(r,\varepsilon_0)^{-b}\varepsilon_0^{\,d} \tag{26}$$

Several rain rates can be associated to Z_α, using (25) with $\delta C=1$. Assuming a constant R-Z relation ($\delta a=1$) yields:

$$R_{ZR}(Z_\alpha) = aZ_m^{\ b}A(r,\varepsilon_0)^{-b} \tag{27}$$

which is the standard version-4 rain rate estimate, $R_{std\text{-}V4}$, for the «true» SR-case.

Similarly, assuming constant k-R relation ($\delta e=1$) yields:

$$R_{kR}(k) = aZ_m^{\ b}A(r)^{-b}\varepsilon_0^{\ d} \tag{28}$$

which is equal to R_C, though Z_C and Z_α are different. In fact, using constant k-R relation is equivalent to adjusting R-Z (by $\delta a=\varepsilon_0^{\ d}$), according to α-adjustment in k-Z (by $\delta\alpha=\varepsilon_0$), in order to keep a self-consistent set of relations via (17). Thus, R_{kR} is formally identical to R_C computed with «unmodified» relations, but with Z_m corrected for a calibration error $\delta C=\varepsilon_0^{-1/\beta}$ (*Marzoug and Amayenc*, 1994, *Iguchi and Meneghini*, 1994; *Tani and Amayenc*, 1998; *Durden et al.*, 1998).

Using N_0^*-scaling in (22) with (16a) for δa , or (16b) for δe, yields:

$$R_{N0} = aZ_m^{\ b}A(r)^{-b}\varepsilon_0^{\ (1-b)/(1-\beta)} \tag{29}$$

Thus, R_{kR}, and R_{N0}, provide *alternative R-estimates to the version-4 standard*, $R_{std\text{-}V4}$. The 3 rain estimates obtainable from α-adjustment are related by:

$$R_{N0} = R_{std\text{-}V4}\,\varepsilon_0^{\ (1-b)/(1-\beta)} \tag{30a}$$

$$R_{kR} = R_{std\text{-}V4}\,\varepsilon_0^{\ d} \tag{30b}$$

With the coefficients used in version 4 (i. e. $\beta= 0.761$, $b\approx 0.65$; $d= b/\beta \approx 0.854$), the rain rate magnitude ranking verifies:

$$R_{N0} \geq R_{kR} \geq R_{std\text{-}V4} \quad \text{for } \varepsilon_0 \geq 1 \text{ , and} \tag{31a}$$

$$R_{N0} \leq R_{kR} \leq R_{std\text{-}V4} \quad \text{for } \varepsilon_0 \leq 1 \tag{31b}$$

As an example, $\varepsilon_0=1.5$ (resp. 0.5) leads to $R_{N0} \approx 1.8$ (resp. 0.36) $R_{std\text{-}V4}$, and $R_{kR} \approx 1.4$ (resp. 0.55) $R_{std\text{-}V4}$, both largely different from the standard $R_{std\text{-}V4}$.

In the hybrid case, identifying ε_f (see (2)) with error terms, which was possible for ε_0 via (19) in the «true» SR-case, is not correct. The mathematical formulation of hybrid estimates involves sophisticated expressions that are not shown here. The important points are: i) the alternative rain estimates are still given by (27), (28), and (29); ii) their ratios still satisfy (30a,b); iii) their relative magnitudes still obey (31a,b), provided that ε_f be substituted for ε_0 in all cases The three R-estimates remain different if $\varepsilon_f \neq 1$.

Using (13), (14), (30a), and (30b), with ε_f instead of ε_0, allows us to compute N_0^*-scaling and alternative R-estimates directly from the output parameter file of the standard version-4 2A-25 *without the need for*

reprocessing. The basic structure of the algorithm, i. e. the attenuation and NUBF corrections, and the corrected Z-profile, are not modified.

The *standard rain estimate of the version-5 2A-25*, $R_{std\text{-}V5}$, based on the N_0-adjustment of *Kozu et al.* (1999), cannot be expressed analytically in a simple manner (see section 3.1).

3.3 Sensitivity of N_0^*-scaling and R-estimates to error sources

N_0^*-scaling can be corrupted by several effects. The «pure» SR-case is required to get an «external» correction factor ε_0 that is first interpretable as $\delta\alpha$-correction in k-Z relation, and then as δN_0^*-correction. Combining (2) and (13) shows that the hybrid scheme, with ε_f instead of ε_0, leads to a hybrid N_0^*-scaling given by:

$$\delta N_0^{*(1-\beta)} = (1-w) + w\, \Delta N_0^{*(1-\beta)} \tag{32}$$

where w is to the same weight as in (2) for ε_f and ΔN_0^* refers to the SR-based correction. Thus, the hybrid δN_0^*-correction, intermediate between 1 (no-correction for the HB-case) and ΔN_0^*- (SR-case), is only an attenuation-dependent weighted fraction of the genuine «true» ΔN_0^*. Also, in essence, α-adjustment ignores error in the radar calibration. Referring again to the SR-case, a calibration error $\delta C \neq 1$ implies $\varepsilon_0 \equiv \delta\alpha\, \delta C^{-\beta} = \delta N_0^{*(1-\beta)}\, \delta C^{-\beta}$. Thus, performing δN_0^*-adjustment while ignoring δC is equivalent to N_0^*-adjustment with

$$\delta N_0^* = \Delta N_0^* \delta C^{-\beta/(1-\beta)} \tag{33}$$

where ΔN_0^*- refers to the «true» N_0^*-correction in absence of calibration error ($\delta C=1$). With $\beta=0.761$ (version-4 2A-25), a calibration offset δC of 1 dB (the typical uncertainty for the TRMM PR) may induce an error of 3.2 dB in the N_0^*-scaling. A third source of error is the uncertainty in the SR itself, i.e. in the experimentally-derived ε_0. This may result, for instance, from changes in surface roughness related to raindrop impacts, or surface wind, over ocean (*Meneghini and Atlas*, 1986). The hybrid scheme usually mitigates this effect except for heavy rain cases (i.e. large PIA) that are highly weighted towards the SR-based solution. NUBF effect may also change the hybrid correction factor ε_f, which has some impact on N_0^*-scaling. This should mainly occur in regions of strong horizontal gradients, like raincell edges. In any case, the NUBF correction scheme in the 2A-25 is expected to decrease the corruption effect. Effects of various types of error on N_0^*-scaling results from TRMM PR data are illustrated in section 4.

The impact of various error sources on the 3 R-estimates can be conveniently evaluated by comparing (27), (28), or (29), with (22) that provides the «true» (though not directly computable) rain rate, R_t. For the SR-case, this yields

$$R_{std\text{-}V4} = \delta C^b\, \delta N_0^{*(b-1)}\, R_t \tag{34a}$$

$$R_{N0} = \delta C^{(b-\beta)/(1-\beta)}\, R_t \tag{34b}$$

$$R_{kR} = \delta N_0^{*(d-1)}\, R_t \tag{34c}$$

which shows how the differences between R-estimates and R_t, depend on the errors δC, and δN_0^*. The additional impact of a possible error δA_t in the SR-based PIA is computed in Appendix 1. Ignoring such an error δA_t, and using β, b, and d values of version-4 yields:

$$R_{std\text{-}V4} = \delta C^{0.65}\, \delta N_0^{*\,-0.35}\, R_t \tag{35a}$$

$$R_{N0} = \delta C^{-0.464}\, R_t \tag{35b}$$

$$R_{kR} = \delta N_0^{*\,-0.146}\, R_t \tag{35c}$$

For the SR-case, via ε_0, the 3 R-estimates have different sensitivities to uncorrected errors. R_{kR}, like the k-estimate, is immune to radar calibration error δC; while $R_{std\text{-}V4}$ and R_{N0}, like the Z-estimate, are not. In essence, R_{N0} is immune to δN_0^* error in the initial relations, and R_{kR} is much less sensitive to δN_0^* than $R_{std\text{-}V4}$, which reflects a well-known feature of rain relations readily obtainable from (10).

These claims have to be somewhat revised for the current case where the 3 R-estimates become sensitive to all error types as a result of hybrid adjustment via ε_F. In particular, R_{N0} (resp. R_{kR}) becomes sensitive to error δN_0^* (resp. δC). It can be shown, however, that: i) R_{N0} and R_{kR} remain less sensitive to errors δC, and δN_0^*, than the standard $R_{std\text{-}V4}$; ii) R_{kR} is less (resp. more) sensitive to error δC (resp. δN_0^*) than R_{N0}.

Therefore, R_{N0} is conceptually the most attractive estimate, but its reliability may be questioned because of potential errors in N_0^*-scaling. For rain estimates that do not use N_0^*-scaling, R_{kR} is expected to be a better candidate than the standard, $R_{std\text{-}V4}$, owing to a lower sensitivity to errors. Comparisons of the three estimates from PR data are discussed in sections 4 and 5. Let us note that, in version-5 2A-25, the N_0-adjustment (*Kozu et al.*, 1999), and the standard rain estimate, $R_{std\text{-}V5}$, are also sensitive to the above-mentioned errors. However, an analytical study of corruption effects by error terms is not achievable.

3.4 Liquid water content estimates

The reasoning followed to get different rain estimates from a set of Z-k-R relations in the framework of version–4 2A-25 can also be utilized to get estimates of the *liquid water concentration* (W) from a set of W-k-Z relations. With help of normalized relations, it was possible to set up W-Z and W-k relations, formally identical to those obtained for R-Z, and R-k, respectively. Using similar hypothesis, and notations, as in the R computations, this led to three possible W-estimates: i) W_{std} as a *standard estimate* based on using constant W-Z relation, ; ii) W_{N0} as an *alternative estimate* based on using N_0^*-scaled W-Z (or equivalently W-k) relation; and iii) W_{kW} as an *alternative estimate* based on using constant W-k relation.

The rain-type-dependent *standard* version-4 W-Z relations were derived from normalized Γ-DSD modeling based on (10) using proper computational parameters: *liquid water*, DSD with μ=1, computation for f=13.8 GHz, temperature in the 0-20°C range, and scaling by rain-type dependent initial N_0^* of the version-4 standard 2A-25 (cf : Table 1). This yields (with W in $g.m^{-3}$, and Z in $mm^6.m^{-3}$):

$$W_{std\text{-}V4} = 3.46 \times 10^{-3}\, Z^{0.545} \quad \text{(for stratiform rain)} \tag{36a}$$

$$W_{std\text{-}V4} = 5.92 \times 10^{-3}\, Z^{0.545} \quad \text{(for convective rain)} \tag{36b}$$

The three W-estimates verify :

$$W_{N0} = W_{std}\, \varepsilon^{(1-b')/(1-\beta)} \tag{37a}$$

$$W_{kW} = W_{std}\, \varepsilon^{d'} \tag{37b}$$

where β, b', and d'(=b'/β) are the coefficients of the $Z=\alpha k^{\beta}$, $W=aZ^{b'}$, and $W=e'k^{d'}$ relations, respectively. Eqs (37a) and (37b) for W are formally identical to (30a) and (30b) for R, respectively.

The version-4 W-estimates are fully consistent with the Z- and R-estimates derived from the PR. Like R-estimates, they can be computed directly from the output file of the version-4 2A-25 without need for reprocessing. A dedicated software has been elaborated to generate easily, for each PR ray path, N_0^*-scaling results, and height-profiles of standard and alternative R and W-estimates. Such ingredients were used in combined PR/TMI rain retrieval algorithms developed by other partners in the framework of the EuroTRMM study.

An «approximate» version-5 W-estimate could also be generated analytically by setting $W_{std\text{-}V5}$-Z relations with rain-type-dependent version-5 initial N_0^* (cf : Table 1). Such relations are formally similar to (36a,b), assuming constant W-Z relation. Getting «true» version-5 estimate should imply to apply directly Kozu's N_0-adjustment (used in version 5) to W-Z relation, which is not available or computable analytically. Results should not be very different as long as $\varepsilon_f \approx 1$.

4. Results of N_0^*-adjustment and rain estimates from PR data

Computation of rain-type dependent N_0^*-scaling and R-estimates were performed for several PR observations. The rain classification involves convective and stratiform rain types, along with «total» rain that refers to the mixing of both rain types without sorting.

4.1 Detailed results in hurricane Bonnie

Detailed results obtained in hurricane Bonnie over Mexico Gulf, as observed on 26 Aug. 1998 (orbit # 4283) during the Convective and Moisture Experiment (CAMEX-3, 1998), are analyzed hereafter. Fig. 3 displays version-4 results of count histograms of ε_f, and $\log(N_0^*)$, for the total rain. The results involve only selected PR beam paths where the SR-based total PIA was judged reliable. Such a criterion, associated in general to PIA>3 dB, provides results significantly weighted towards the SR-based solution. The ε_f-distribution reaches a maximum for $\varepsilon_f > 1$, with a mean of 1.561, and a standard deviation of 0.195. The associated distribution of δN_0^* (not shown), from (13), also peaks for $\delta N_0^* > 1$. The mean adjusted N_0^* is higher than the initial value, by a factor of about 4.

The rain-type dependent means of ε_f, and $\langle N_0^* \rangle / N_{0\,init}^*$, are summarized in Table 2 for the selected PR beam paths, and for the case involving all PR beam paths (note that the number of involved paths is largely increased). The standard deviation of ε_f, the areal mean of the standard rain rate ($\langle R_{std\text{-}V4} \rangle$), and the ratio of each alternative rain rate ($\langle R_{N0} \rangle$ or $\langle R_{kR} \rangle$) to the standard, at 2-km height, are also listed. At this altitude, the rain signal is not contaminated by surface clutter at off-nadir beam incidences. In all cases, $\langle \varepsilon_f \rangle$ exceeds unity, the adjusted $\langle N_0^* \rangle$ exceeds the initial value, and the alternative rain rates (with $\langle R_{N0} \rangle$ the largest) are higher than the standard. All these deviations increase when going from the full-hybrid solution (all PIA) to the SR-weighted case (reliable PIA only). Ideally, the algorithm should provide ε_f-distribution with $\langle \varepsilon_f \rangle \approx 1$, and a small std dev. around the mean. The fact that $\langle \varepsilon_f \rangle$ is preponderantly larger than unity implies a systematic adjustment of the k-Z relation, in such a way that the PIA correction is increased with respect to the HB-based estimate (see (20)). Correlatively, obtaining $\langle N_0^* \rangle$ usually greater than the initial value implies that initial N_0^* is ill-adapted and/or N_0^*-scaling is possibly contaminated by unknown error terms.

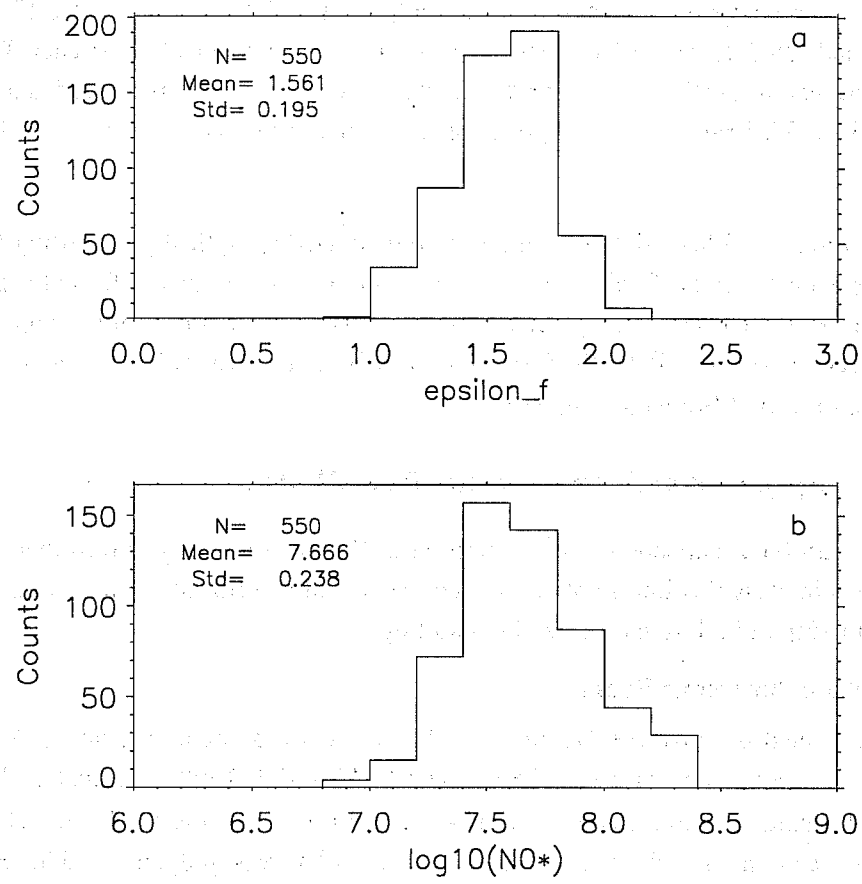

Fig. 3: Count histograms of ***a)*** ε_f *and* ***b)*** *adjusted* $\log(N_0^*)$*, as derived from the version-4 2A-25 hybrid algorithm, in hurricane Bonnie (26 Aug. 1998, orbit # 4283). Results refer to total rain, and selected PR beam paths with reliable SR-based total PIA. The initial* N_0^* *(*10.9×10^6 m^{-4}*) corresponds to* $\log(N_0^*) = 7.037$.

Parameter	All paths			Paths with reliable PIA_s only		
	S-Rain	C-rain	T-rain	S-rain	C-rain	T-rain
$\langle\varepsilon_f\rangle$	1.243	1.304	1.249	1.624	1.445	1.561
Std dev of ε_f	0.359	0.289	0.353	0.178	0.223	0.195
$N_{0\ init}^*$ ($\times 10^6$ m^{-4}	5.1	16.6	10.9	5.1	16.6	10.9
$\langle N_0^* \rangle / N_{0\ init}^*$	2.0	2.79	1.09	6.98	4.53	4.25
$\langle R_{STD\text{-}V4} \rangle$(mm h^{-1})	2.2	12.1	3.3	5.9	17.4	10.0
$\langle R_{N0} \rangle / \langle R_{std\text{-}V4} \rangle$	1.53	1.56	1.55	2.05	1.67	1.82
$\langle R_{kR} \rangle / \langle R_{std\text{-}V4} \rangle$	1.27	1.28	1.27	1.52	1.34	1.41
Number of paths	2997	336	3333	356	194	550

Table 2: Mean value of ε_f *(and the standard deviation from the mean),* $N_0^*/N_{0\ init}^*$*,* $R_{std\text{-}V4}$*; and the ratio of each alternative (*R_{N0} *or* R_{kR}*) to the standard rain rate, for stratiform (S), convective, (C), and total (T) rain, as derived from version-4 2A-25 in hurricane Bonnie (26 Aug. 1998, orbit # 4283). Rain rates refer to a 2-km altitude.* $N_{0\ init}^*$ *stands for initial* N_0^* *(cf: Table 1), and* PIA_s *is the SR-based total PIA.*

Fig. 4 points out how the retrieved rain-type dependent $<N_0^*>$ from version 4 changes with respect to errors/effects that were discussed in section 3.3. The standard hybrid algorithm results, for all PR beam

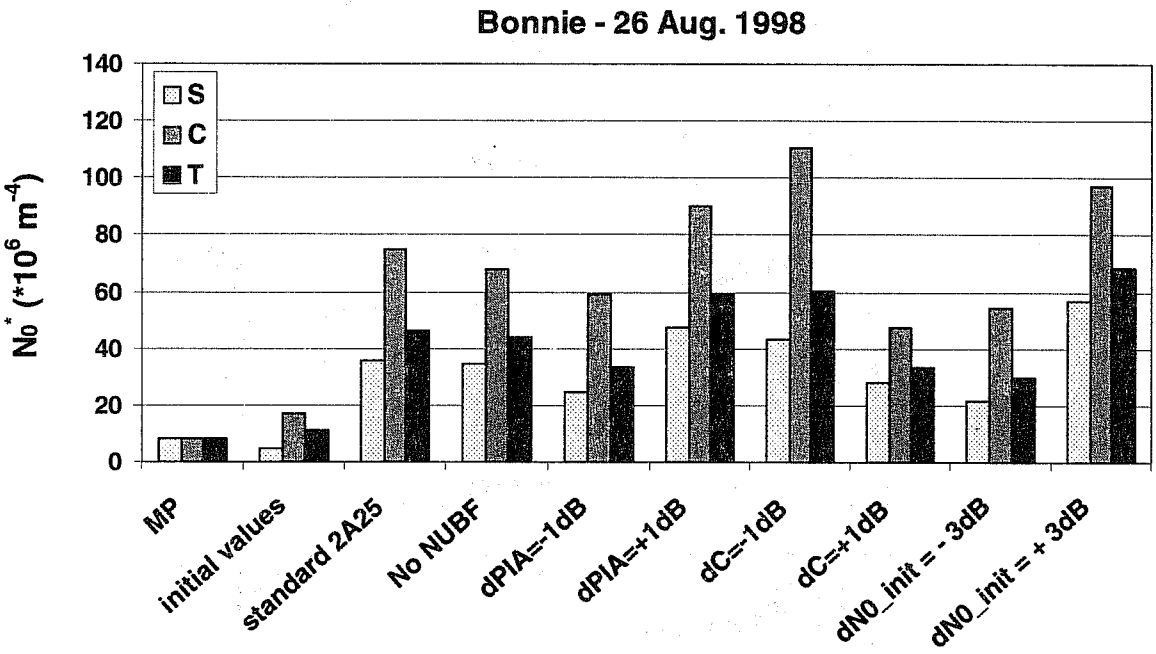

Fig. 4: From left to right: Marshall-Palmer N_0^* (MP); and initial N_0^* in the version-4 2A-25. Then, for Bonnie hurricane, adjusted $<N_0^*>$ derived from the standard hybrid 2A-25 (reference case); adjusted $<N_0^*>$ after cancelling NUBF correction; adjusted $<N_0^*>$ in the presence of simulated bias in SR-based total PIA (± 1 dB), radar calibration (± 1 dB), and initial N_0^* (± 3 dB), respectively. Every column diagram shows results for convective (C), stratiform (S), and total (T) rain.

paths, were considered as reference for comparisons. Then, the algorithm was reprocessed, after simulating separately some specific error/effect. First, the stability of N_0^*-scaling results with respect to spatial sampling was checked by processing separately PR data included in the right-hand side, or the left-hand side half-swath, and comparing them with the full-swath case. $<N_0^*>$ results (not shown) for the three configurations differ by less than 10%. NUBF effects have low impact on N_0^*-scaling, especially for stratiform rain, since suppressing the NUBF correction in the simulation changes $<N_0^*>$ by less than 15%. Adding a constant bias in the SR-based total PIA (±1 dB), radar calibration (±1 dB), or initial N_0^* (±3 dB), may change the results by a factor of 2 with respect to the reference case. The sensitivity of N_0^* to an offset δN_0^* in $N_{0\,init}^*$ is partly governed by the hybrid character of the adjustment (see section 3.3). This prevents the offset in question to be compensated for in the retrieved $<N_0^*>$, as it would be for a «true» SR-based solution. The impact of errors amplifies when restricting the analysis to selected paths with significant SR-weighting, except for δN_0^*-error that is better corrected via N_0^*-adjustment.

Results from version 5 are shown in Table 3, like in Table 2 for version 4, except that the last two lines refer now to the areal mean of the standard version-5 rain rate ($<R_{std\text{-}V5}>$), and the ratio $<R_{std\text{-}V5}>/<R_{std\text{-}V4}>$. Comparison with version-4 results shows that $<\varepsilon_f>$ for each category is much closer to unity, and the std dev. of ε_f is strongly reduced, especially for «all paths» case. Meanwhile, the adjusted mean $<N_0^*>$ is closer to initial $N_{0\,init}^*$, in all cases. Besides, $<R_{std\text{-}V5}>$ is always larger than $<R_{std\text{-}V4}>$. Note that the number of paths in each category is slightly different for the two versions.

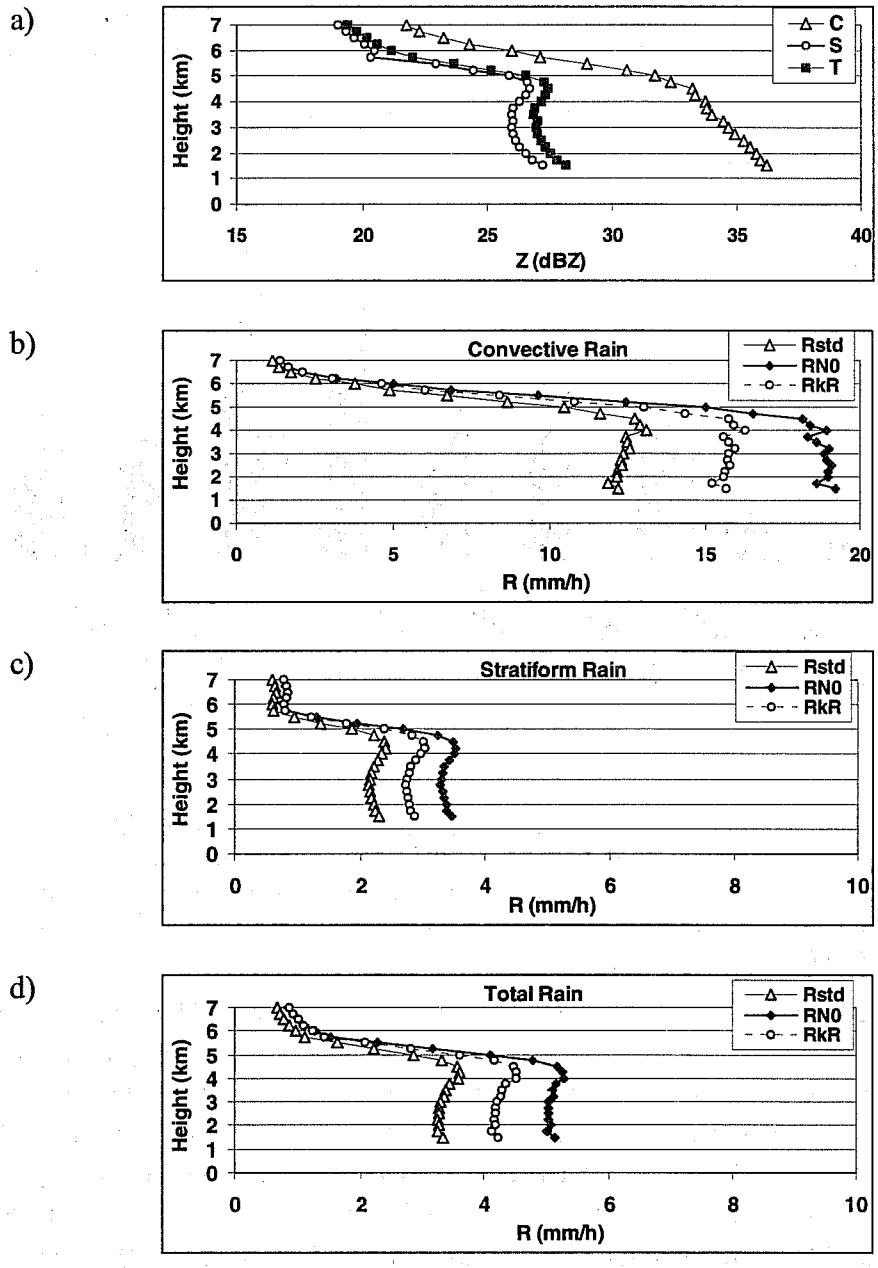

Fig. 5: Height-profile, above 1.5-km height, of mean parameters horizontally-averaged over the Bonnie hurricane area for all TRMM PR beam paths, as derived from the version-4 2A-25 algorithm: a) reflectivity factor for various rain types; and rain rates for b) convective (C) rain, c) stratiform (S) rain, and d) total (T) rain. Panels b to d include the standard estimate, $R_{std\text{-}V4}$; and the alternative estimates, R_{N0}, and R_{kR}. Note the change in horizontal scale in panels c, and d, with respect to panel b.

Fig. 5a displays height-profiles of the mean reflectivity factor, <Z>, retrieved in Bonnie from the version-4 standard 2A-25 algorithm above 1.5-km height, for each rain type. The <Z>-profile for total rain (no sorting versus rain type) looks like the stratiform profile, owing to the prevailing number paths in stratiform rain (cf: Table 2). Height-profiles of the three mean rain rates are shown in Figs. 5b,c,d. Differences between the alternative rain rates and the standard one, in the rain region (below 4.5-km height), are almost constant versus height, whatever the rain type. The alternative rain rates are higher than the standard $<R_{std\text{-}V4}>$ by about 50% (resp. 30%) for $<R_{N0}>$ (resp. $<R_{kR}>$), for all rain types. Fig. 6a (resp. Fig. 6b,c,d displays height-profiles of <Z> (resp. <R>) retrieved from version-5 standard 2A-25. Height-profiles of <Z>, and <R>, respectively, have similar shapes to their version-4 counterparts (Fig . 5), for

each rain type. However, <Z> is larger by about 0.5 dB, which is mainly a result of change in the radar calibration (see section 2.2); and $<R_{std\text{-}V5}>$ exceeds $<R_{std\text{-}V4}>$ by about 15% for convective rain, and 30% for stratiform or total rain. Fig 7 displays the standard version-4 rain rate field ($R_{sd\text{-}V4}$) retrieved at 2-km height. The rain patterns from all other R-estimates (not shown) are quite similar despite differences in rain rate magnitudes.

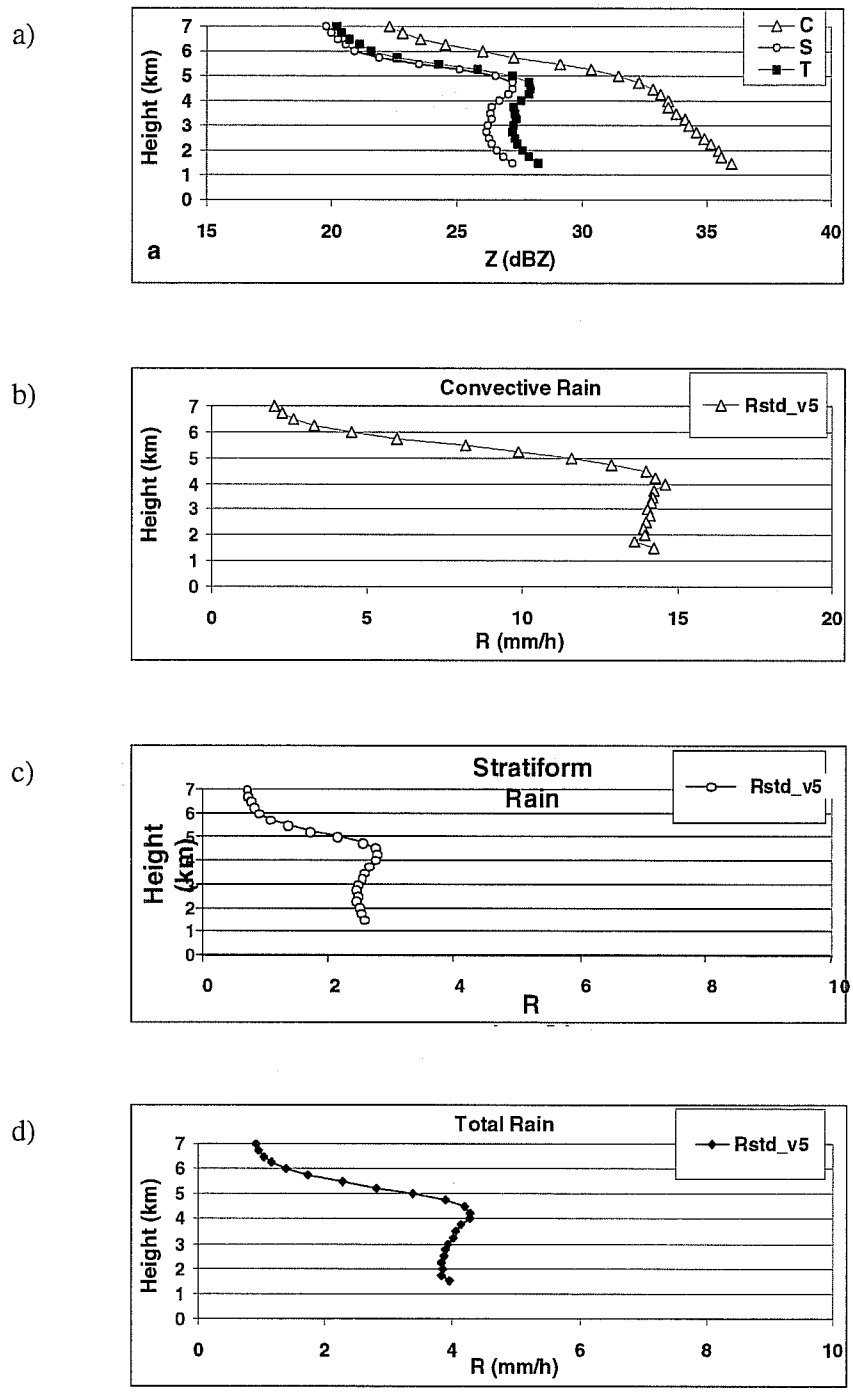

Fig. 6: Same as Fig. 5, but for the version-5 standard 2A-25 algorithm. Panels b to d refer to the version-5 standard estimate, $R_{std\text{-}V5}$, only

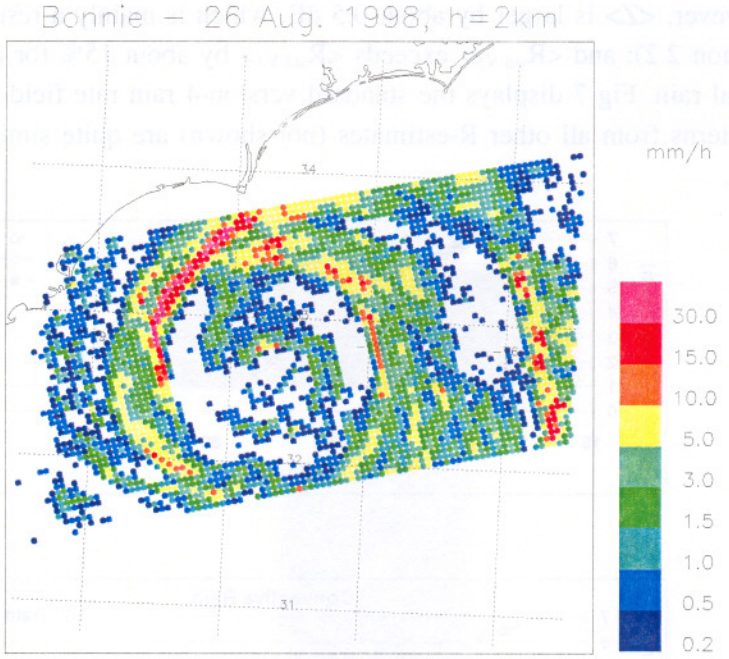

Fig. 7: Rain rate fields at 2-km height, provided by the standard estimate, $R_{std\text{-}V4}$, of the version-4 2A-25 hybrid algorithm, in hurricane Bonnie (26 Aug. 1998, orbit # 4283). The pattern is shown in the PR swath, with indication of the latitude-longitude frame.

The bulk characteristics pointed out in N_0^*-scaling and R-estimate results (for both versions of the algorithm) also emerge from the analysis of a larger PR data set in section 4.2.

Parameter	All paths			Paths with reliable PIA_s only		
	S-Rain	C-rain	T-rain	S-rain	C-rain	T-rain
$\langle\varepsilon_f\rangle$	1.002	1.038	1.006	1.021	1.067	1.042
Std dev of ε_f	0.014	0.095	0.036	0.044	0.118	0.089
$N_{0\ init}^*$ ($\times 10^6$ m^{-4})	7.4	15.7	11.6	7.4	15.7	11.6
$\langle N_0^* \rangle / N_{0\ init}^*$	1.01	1.25	1.04	1.11	1.43	1.25
$\langle R_{STD\text{-}V5} \rangle$ (mm h^{-1})	2.9	13.8	4.4	8.3	20.9	14.0
$\langle R_{std\text{-}V5} \rangle / \langle R_{std\text{-}V4} \rangle$	1.32	1.14	1.33	1.41	1.20	1.40
Number of paths	2371	379	2750	263	215	478

Table 3: Mean value of ε_f (and the standard deviation from the mean), $N_0^*/N_{0\ init}^*$, $R_{std\text{-}V5}$, and the ratio $R_{std\text{-}V5}/R_{std\text{-}V4}$, for stratiform (S), convective, (C), and total (T) rain, as derived from version-5 2A-25 in hurricane Bonnie (26 Aug. 1998, orbit # 4283). Rain rates refer to a 2-km altitude. $N_{0\ init}^*$ stands for initial N_0^* (cf: Table 1), and PIA_s is the SR-based total PIA.

4.2 Statistics of PR-derived results for a set of events

N_0^*-scaling and R-estimates computations were performed for 13 TRMM PR observations in various meteorological conditions over ocean (9 cases), and land (4 cases), listed in Table 4. The case of hurricane Brett, further involved in the study (see section 5) is not included, because version-4 data were not available for this event.

Fig. 8 shows, for all events and rain types, the mean parameters obtained from version 4: the hybrid correction factor $\langle\varepsilon_f\rangle$; the ratio $\langle N_0^* \rangle / N_{0\ init}^*$; the standard rain estimate, $\langle R_{std\text{-}V4} \rangle$; and the ratio of each alternative estimate to the standard, $\langle R_{N0} \rangle / \langle R_{std\text{-}V4} \rangle$, and $\langle R_{kR} \rangle / \langle R_{std\text{-}V4} \rangle$, at 2-km height. For all events,

$<\varepsilon_f>$ is greater than 1. Typically, $<\varepsilon_f> \approx 1.2$ to 1.4. The sample means are close to 1.3. Consequently, $<N_0^*>/N_{0\,init}^*$ is larger than 1 for each rain type; and may reach a value of 3. For total rain, however, it does not exceed 1.8 owing to the fact that the reference $N_{0\,init}^*$ is defined as the mean of the stratiform and convective rain cases. The ratio would increase if $N_{0\,init}^*$, like $<N_0^*>$, involved weighting by the relative numbers of PR beam paths in stratiform and convective rain. Referring to $<R_{std\text{-}V4}>$ for each event/rain-type, $<R_{N0}>/<R_{std\text{-}V4}>$ ranges from 1.35 to 1.8, and $<R_{kR}>/<R_{std\text{-}V4}>$ from 1.18 to 1.4. For all rain types, the sample mean of the ratio is close to 1.5 for $<R_{N0}>$, and 1.25 for $<R_{kR}>$. On average, the systematic tendency for N_0^* to be adjusted to values higher than $N_{0\,init}^*$, and for the R-estimates to satisfy the inequalities $R_{N0}>R_{kR}>R_{std\text{-}V4}$, is confirmed.

Case	Date	Orbit #	Location	Type of event
1	08 26 1998	4283	Mexico Gulf	Hurricane Bonnie
2	08 26 1998	4285	id°	Hurricane Bonnie
3	09 19 1998	4656	id°	Hurricane Georges
4	01 27 1998	0952	Over Darwin site	Convection lines (land)
5	01 25 1998	0921	Near Darwin site	Mainly stratiform rain (land)
6	01 25 1998	0930	id°	Spotty convection (land)
7	01 19 1998	0837	id°	Convection lines
8	01 01 1998	0544	id°	Spotty convection (land)
9	02 01 1998	1033	West Pacific	Mainly stratiform rain
10	08 07 1998	3976	Central Pacific	Line-organized convection
11	08 08 1998	3991	id°	Spotty convection
12	08 09 1998	4021	id°	Organized MCC
13	08 13 1998	4074	id°	Large bow-shaped MCC

Table 4: The 13 PR observations, and their main characteristics, involved in the results of Fig. 8. MCC stands for mesoscale convective complex. All observations are made over ocean except 4, 5, 6, and 8, made over land.

Fig. 9 shows similar results for version-5, except that the last two plots at bottom display now $<R_{std\text{-}V5}>$, and the ratio $<R_{std\text{-}V5}>/<R_{std\text{-}V4}>$. Comparison with results of Fig. 8 for version 4 shows that, for all events and rain types, $<\varepsilon_f>$ (ranging from 1 to 1.07) is closer to 1; also, the std dev. from the mean (not shown) is reduced by a large factor. All sample means are close to 1. Correlatively, $<N_0^*>$ (not used in the frame of version-5 data) is closer to the initial $N_{0\,init}^*$, in all cases. Such changes likely result from the improved computation of ε_f, and/or a better-adapted initial k-Z relation in version 5 (see section 2.2). They clearly point out a better functioning of the version-5 algorithm. Meanwhile, observing $<R_{std\text{-}V5}>/<R_{std\text{-}V4}>$ above unity in all cases confirms a systematic increase in rain rate estimates from version 4 to version 5. This relative increase is smaller for convective rain (sample mean ≈ 1.2) than for stratiform or total rain (sample means ≈ 1.3), except for event #2.

In contrast to the findings of *Iguchi et al.* (2000) from results of the version-5 standard, differences between data over ocean or land (events 4 to 6, and 8) are not evident. However, all "land" cases refer to data taken in the vicinity of Darwin site (Australia) during the wet season. This site is likely not well representative of typical continental conditions for the observed storms.

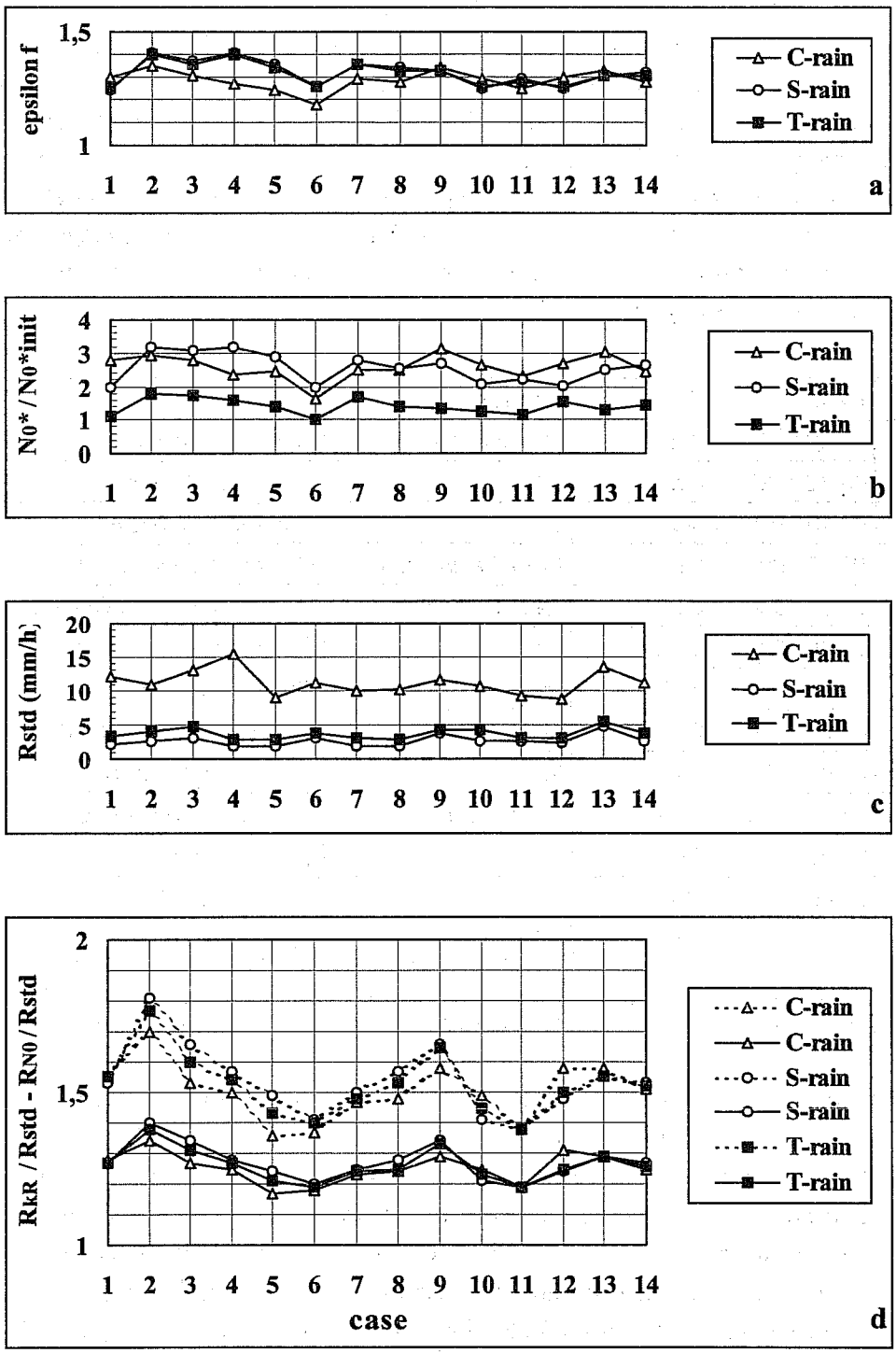

Fig. 8: For 13 cases of TRMM PR observations (see Table 4): mean values of a) the hybrid correction factor ε_f; b) the ratio of adjusted N_0^* to initial N_0^* (see Table 1); c) the standard rain rate, R_{std-4}, at 2-km height; and d) the ratio of each alternative rain rate estimate (R_{N0} or R_{kR}) to the standard, at 2-km height. All results, computed in the frame of the version-4 hybrid 2A-25 algorithm, are shown for convective (C), stratiform (S), and total (T) rain. For each plot, the sample mean, quoted case 14, is also indicated. Data points are linked by segments to better vizualize case-to-case changes in the results.

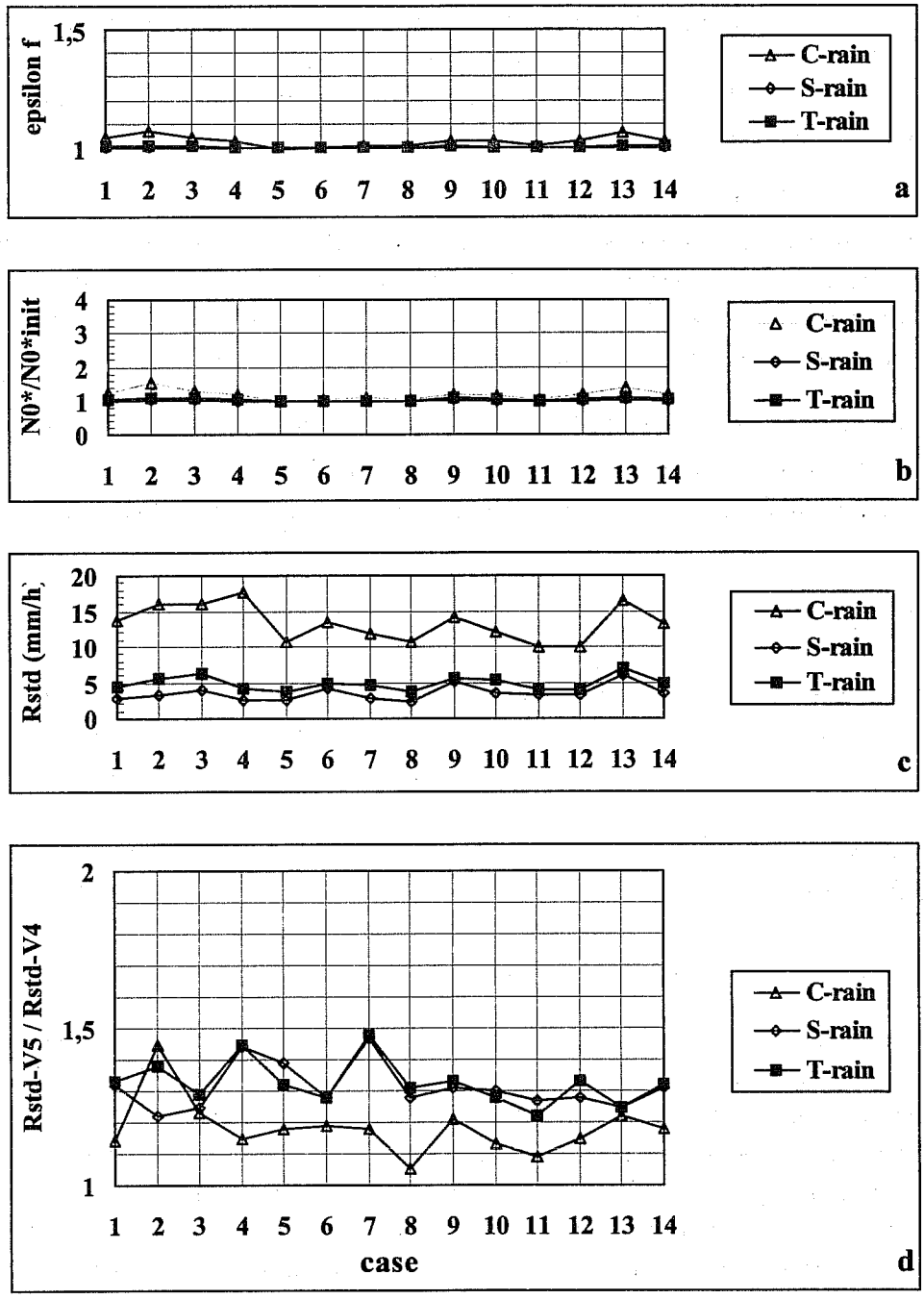

Fig. 9: Same as Fig. 8, but for version-5 standard results. Besides, the bottom plot (d) is the ratio of the standard version-5 ($R_{std\text{-}V5}$) to the standard version-4 ($R_{std\text{-}V4}$) rain estimate.

5. Tests of PR-derived rain parameters using coincident airborne radar data

Rain products derived from the TRMM PR can be tested by comparing them with external data taken as reference eventhough no rain measurement of any kind can be considered as "truth". For this purpose, small-scale rain obervations over large areas from ground-based, or airborne radar are quite useful provided that data sets be acquired in "good" space/time coincidence with PR data. In this section, we report comparison results based upon the use of data gathered by the Doppler dual-beam X-band radar on board NOAA/P3 aircraft, in hurricanes Bonnie and Brett. In each case, the P3-radar data were acquired in combination with a TRMM overpass, that occurred at 1137 UT on 26 Aug. 1998 (orbit #4283) for Bonnie,

and at 2240 UT on 21 Aug. 99 (orbit #9967) for Brett, over Mexico Gulf. These are the best cases that we could select. Good coincidence between the P3-radar and PR observations allowed us performing point-to point comparisons of retrieved Z- and R-fields. Version-4 (for Bonnie, only), and version-5 (for Bonnie and Brett) PR data were available for comparisons.

5.1 Processing of the P3-radar data

A four-step procedure was used to process the P3-radar data, including: i) the correction of apparent Z_m-field for path-attenuation, then for error in the radar calibration; ii) the correction of Z-field for advection effects; iii) the computation of the «reference» Z-field (Z_{P3}) by averaging at the PR beam resolution, and iv) the computation of the «reference» rain rate field (R_{P3}).

The measured reflectivity Z_m-field of the P3-radar was corrected for path attenuation using the "hybrid" stereoradar/dual-beam algorithm (*Oury et al.*, 1998, *Oury et al.*, 2000). The *absolute error* in the radar calibration, ΔC, which may induce large bias in the R-retrieval, was corrected according to *Oury et al* (2000), as:

$$\Delta C = -10\log(\alpha/\alpha_0)/\beta \tag{38}$$

where α is the coefficient of the $k=\alpha Z^\beta$ relation at X-band provided by the analysis, and α_0 is a reference value computed from a N_0^*-scaled k-Z relation derived from a microphysical model. This model involves normalized DSD adapted to experiment conditions encountered in P3-radar measurements, i.e. X-band, vertical polarization, and nearly horizontal viewing of oblate raindrops. The k-Z relation was scaled by initial N_0^* for convective rain in the 2A-25 algorithm (cf: Table 1) since P3-data analysis mainly relies on cases with significant path-attenuation to get ΔC. Note that changing N_0^* by 50% modifies ΔC by 0.5 dB; and increasing (resp. decreasing) N_0^* yields larger (resp. smaller) Z. The above procedure provides Z-fields from P3-radar that are corrected for path-attenuation effects, and calibration error.

The typical sampling time of a hurricane by the airborne P3-radar is about one hour owing to the aircraft flight speed of 120 m s^{-1}, while it is one-to-two minutes for the TRMM PR. Therefore, the nearly instantaneous rain pattern depicted by the PR may evolve and move during the airborne radar sampling time. Such an effect was hopefully reduced by restricting the region used for comparisons to a domain where the maximum time lag between the two samplings did not exceed 10 min. Also, the rain pattern was corrected for advection using a model for the horizontal tangential speed (V_t in m s^{-1}) of individual rain cells versus the radial distance (d in km) to the eye center (F. Marks, private communication):

$$V_t = 9.338 + 6.407 \times 10^{-2} d + 1.2676 \times 10^{-2} d^2 - 1.5856 \times 10^{-4} d^3 + 6.4171 \times 10^{-7} d^4 - 8.517 \times 10^{-7} d^5 \tag{39}$$

Considering the "degraded" PR cross-range resolution ($\approx$ 4.2 km in nearly horizontal plane at 350 km range) with respect to that of the P3-radar ($\approx$1.6 km in horizontal direction, for an involved typical maximum range of 50 km), a PR beam-like smoothing was applied to P3-radar data in order to get significant comparisons of Z from both instruments. Accordingly, Z fields retrieved from the P3-radar were interpolated horizontally on the PR grid, then averaged with a Gaussian beam-weighting gain function, $P(\rho)=\exp[-2 \ln 2 (\rho/\rho_0)^2]$, where $2\rho_0$=4.2-km is the PR half-power cross-range resolution, and ρ is the radial distance of any involved P3-radar data point to the nearest data point of the PR grid. Difference in the PR vertical resolution (250 m) and the equivalent vertical resolution of the P3-radar was ignored.

For computing the P3-radar "reference" R-field, the vertical storm structure depending on the PR-derived rain-type, and the R-Z relationships in ice, were taken similar to those used in the 2A-25, for self-consistency. In rain, R-field was derived from Z-field using rain type dependent N_0^*-scaled normalized relations $R= aN_0^{*(1-b)}Z^b$. Coefficients a and b were taken as representative of the P3-radar experiment conditions (frequency, polarization, and viewing geometry); and N_0^* was taken equal to the initial value used in the 2A-25 for stratiform or convective rain type (cf: Table 1), as categorized by the PR. Of course, this assumes that the PR and P3-radar data are perfectly co-located in space and time. The final R was corrected for change in air density with height according to *Foote and du Toit* (1969).

5.2 Analysis of TRMM PR/P3-radar comparison results in hurricane Bonnie

Horizontal cross-section, at 2.8-km height, of raw «apparent» reflectivities, Z_m, measured by the TRMM PR and P3-radar in Bonnie are shown in Fig. 10. The P3-radar Z_m-field (Fig. 10a) is underestimated when compared to the PR-derived one (Fig. 10b). The P3-radar calibration correction, derived from (38), leads to increase Z_m by 6.5 dB. Z-fields corrected for calibration error, and for path-attenuation (version-4 2A-25 for the PR), are displayed in Figs. 10c,d. The two P3-radar fields in Figs. 10a,c are corrected for advection, and the corrected Z-field is averaged at the PR beam resolution in Fig. 10c. Both corrected Z-fields agree much better.

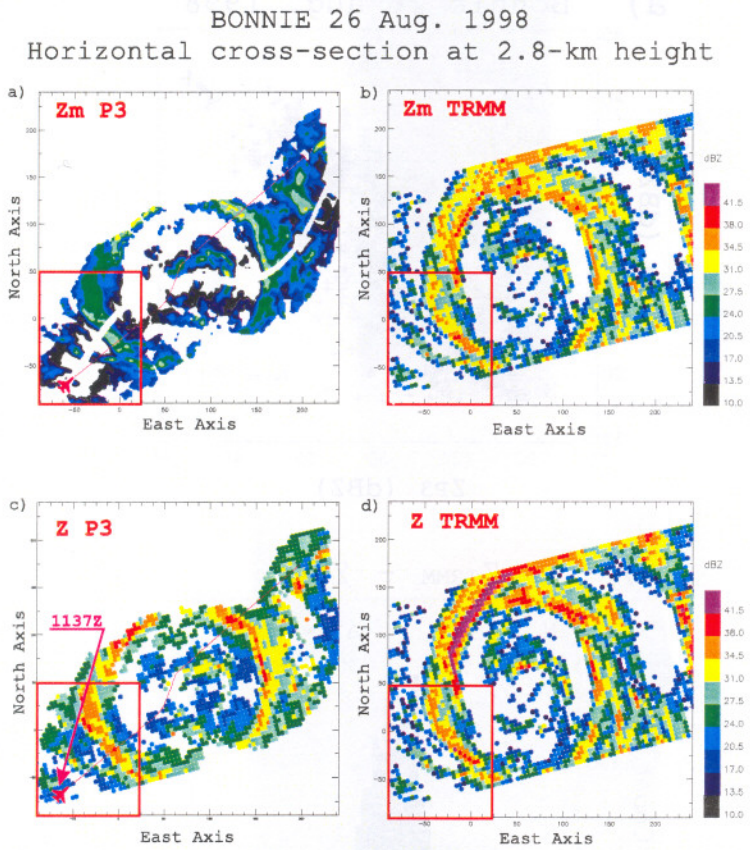

Fig. 10: For hurricane Bonnie, horizontal cross-section of the reflectivity fields at 2.8-km height: a) apparent reflectivity, Z_m, measured by the P3-radar; b) apparent reflectivity, Z_m, measured by the TRMM PR (26 Aug. 1998, orbit # 4283); c) P3-radar reflectivity, Z_{P3}, corrected for attenuation, and radar calibration error; d) TRMM PR attenuation-corrected reflectivity, Z_{TRMM}, from the version-4 2A-25 algorithm. The P3–radar fields, in panels a and c, are corrected for advection. The P3-radar field, in panel c, is averaged at the PR beam resolution. The box at left bottom delineates the domain used for point-to-point comparisons. The genuine flight-track of the P3-42 aircraft is indicated in panel a.

The «comparison domain» (≈100 x 100 km^2) is also drawn. Outside this domain, a large part of the hurricane (where the time lag between the two samplings exceeds 10 min) could be used for point-to-point comparisons. Besides, the small number of paths in convective rain in the comparison domain prevented us from collecting reliable results for this rain type. Thus, the following results refer to total (mostly stratiform) rain, only.

A comparison of 3-D corrected reflectivities of the PR (version 4) and P3-radar, for all data points within the [2-4] km height range in the comparison domain, is shown in the scatter plot of Fig. 11a. The comparison involves only points where Z is above the PR detection threshold (18 dBZ). The associated histogram of differences, $\Delta Z = (Z_{TRMM}-Z_{P3})$, displayed in Fig. 11b, is sharply-peaked. As seen in Table 5, the mean difference is small: $\langle\Delta Z\rangle$= -0.7 dB with a std dev. σ_Z=4 dB (for 1817 data points) for version-4 results; and $\langle\Delta Z\rangle$= -0.2 dB with σ_Z=4 dB (for 1765 data points) for version-5 results. The 0.5-dB shift likely reflects the change of 0.52 dB in the PR calibration in version 5 (cf: section 2.2). Thus, <Z> retrieved from the PR, for both versions, is slightly lower than <Z> retrieved from P3-radar. This feature is almost constant with height in the rain zone (below 4 km), as shown by the mean horizontally-averaged vertical Z-profiles in Fig. 12.

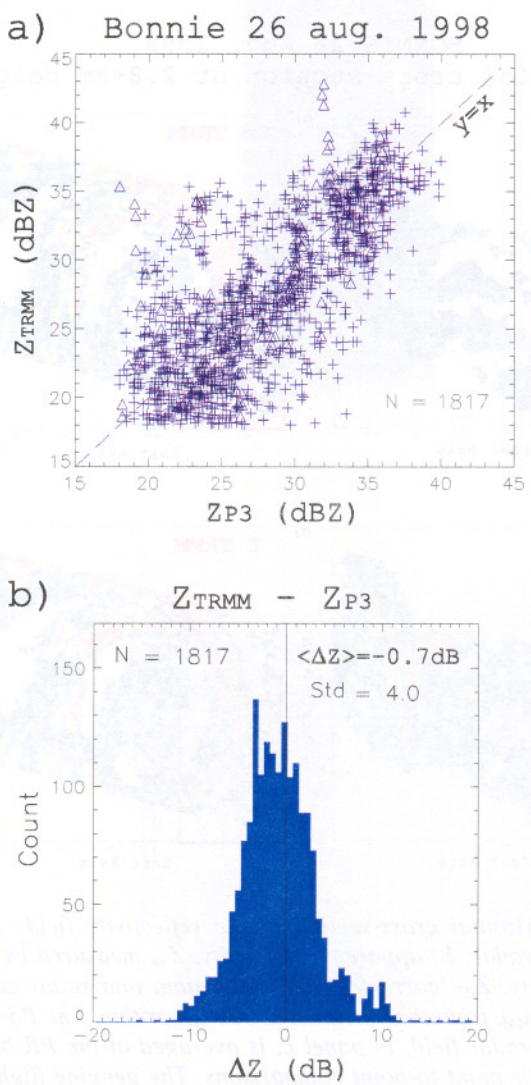

Fig. 11: Comparison of corrected Z retrieved from the TRMM PR and P3-radar, for all data points within the [2-4] km height range in the comparison domain for Bonnie (see Fig. 10): a) Z_{TRMM} (version 4) versus Z_{P3}, with symbol + (resp. triangle) for stratiform (resp. convective) rain; b) related histogram of $(Z_{TRMM}-Z_{P3})$ differences, for total rain.

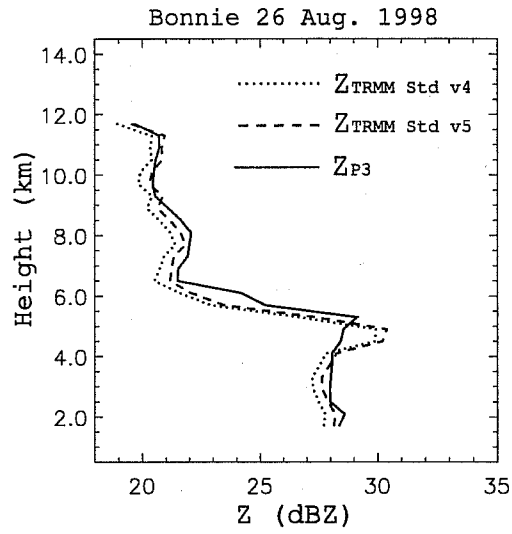

Fig. 12: Mean vertical profiles of horizontally-averaged corrected reflectivity factor $<Z_{TRMM}>$ (versions 4 and 5), and $<Z_{P3}>$, for total rain, in the compaison domain for Bonnie.

It is not expected that $<\Delta Z>$ be zero owing to differences in frequencies (X- and K_u-bands), and scanning geometries, for both instruments. A simple data-based model of the expected difference $<\Delta Z>_{th}$, and the std dev. $\sigma_{Z,th}$, is described in Appendix 2. The model predicts a positive difference, $<\Delta Z>_{th} \approx +1$ dB, i.e. PR value above the P3-radar one. The observed $<\Delta Z>$ (-0.7 dB for version 4, and -0.2 dB for version 5) is slightly different; the best agreement is obtained for version-5. Anyway, the 1.7-dB (resp. 1.2-dB) offset from theory for version 4 (resp. version 5) is compatible with the uncertainty margin (≈2 dB) due to residual calibration errors of both radars (about 1 dB for each one). The observed large std dev. (σ_Z= 4 dB) compared with theory ($\sigma_{Z,th} \approx$ 0.2 dB) may come from combined effects of measurement noise, residual uncertainties in data co-locations, and evolution/advection of the hurricane structure during the P3-radar sampling time.

The mean (horizontally-averaged) vertical R-profiles retrieved from the PR, and P3-radar (R_{P3}), are shown in Fig. 13. The mean differences, standard deviations, and ratios of all PR-derived estimates with respect to the P3 "reference", $<R_{P3}>$= 3.4 mm h^{-1}, in the [2-4] height range, are listed in Table 5. Histograms of point-to point differences in the 2-4 km height range, for the alternative version-4 estimate R_{kR}, and the version-5 standard $R_{std\text{-}V5}$, which are the best two cases, are shown in Fig. 14. The version-4 alternative estimates, R_{kR}, and R_{N0}, are larger than the standard $R_{std\text{-}V4}$, by 19%, and 39%, respectively; in accordance with previous findings (see section 4). Also, the standard $R_{std\text{-}V5}$ is higher than $R_{std\text{-}V4}$ by 15%. Clearly, R_{kR}, and $R_{std\text{-}V5}$, show the best agreement with the "reference" R_{P3} (within 5 %, and 8%, margin, respectively) while $R_{std\text{-}V4}$ (resp. R_{N0}) underestimates (resp. overestimates) R_{P3} by 20% (resp. 12%). Therefore, the reported deficiency of $R_{std\text{-}V4}$ seems rather well alleviated by the alternative version-4 estimate R_{kR}, or the standard version-5 estimate $R_{std\text{-}V5}$.

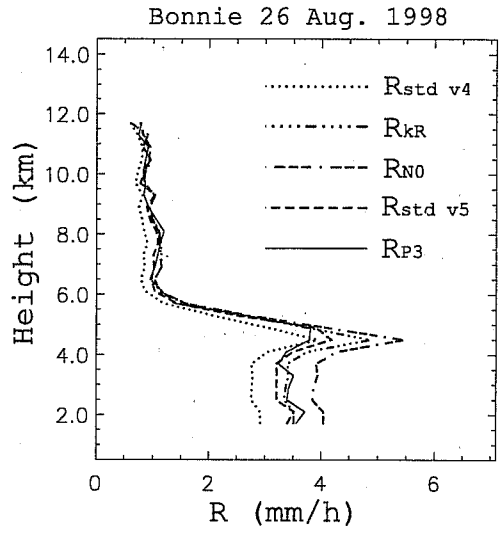

Fig. 13: Mean vertical profiles of horizontally-averaged rain rates in the comparison domain for Bonnie. The rain rates refer to total rain, for the TRMM PR estimates ($R_{std\text{-}V4}$, R_{kR}, and R_{N0} for version 4; and the version-5 standard $R_{std\text{-}V5}$), and the P3-radar estimate (R_{P3}).

Parameter	<Mean>	Std dev.
$(Z_{TRMM}-Z_{P3})$ for V4 (dB)	-0.7	4
$(Z_{TRMM}-Z_{P3})$ for V5 (dB)	-0.2	4
$(R_{std\text{-}V4}-R_{P3})$ (mm/h)	-0.6	2
$(R_{kR}-R_{P3})$ (mm/h)	-0.1	2.4
$(R_{N0}-R_{P3})$ (mm/h)	0.4	2.7
$(R_{std\text{-}V5}-R_{P3})$ (mm/h)	-0.2	2.3
$<R_{P3}>$ (mm/h)	3.4	-
$<R_{std\text{-}V4}> / <R_{P3}>$	**0.80**	-
$<R_{kR}> / <R_{P3}>$	**0.95**	-
$<R_{N0}> / <R_{P3}>$	**1.12**	-
$<R_{std\text{-}V5}> / <R_{P3}>$	**0.92**	-

Table 5: Z-, and R-estimates, from the TRMM PR and P3-radar, in the comparison domain of hurricane Bonnie (see Fig. 10). The results refer to all data points within the [2-4] km height range, and total rain.

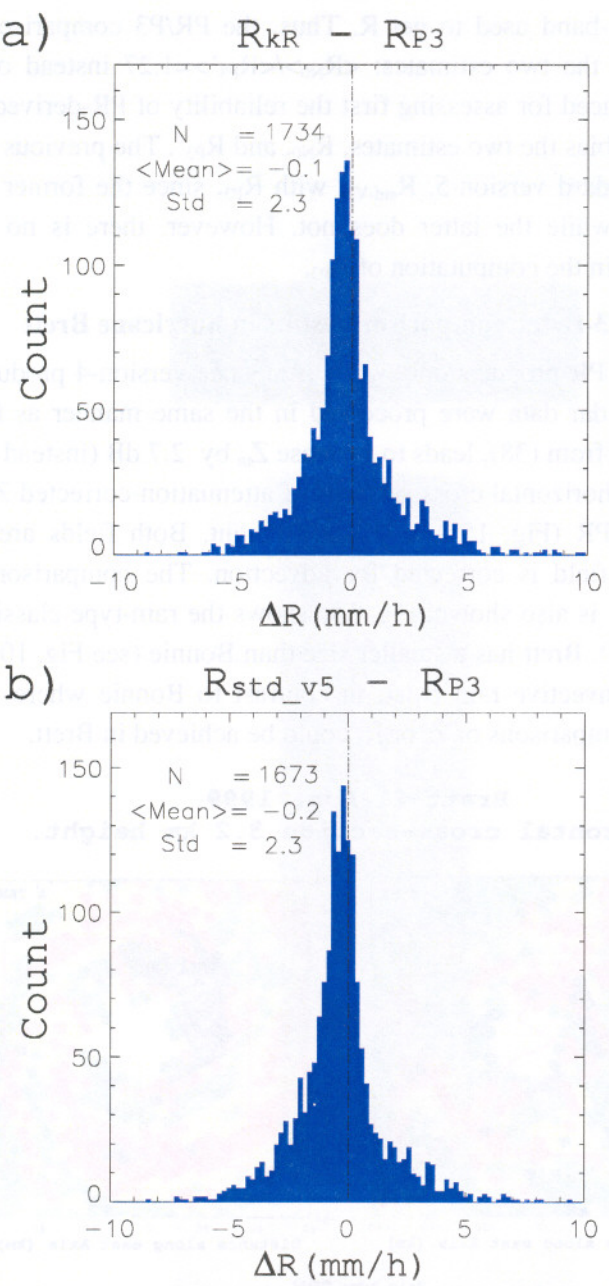

Fig. 14: Histograms of rain rate differences, (R_{TRMM}-R_{P3}), for all data points within the [2-4] km height range, and for total rain, in the comparison domain for Bonnie. R_{TRMM} stands for: a) the TRMM PR-derived version-4 alternative rain rate, R_{kR}; and b) the version-5 standard rain rate, $R_{std\text{-}V5}$. R_{P3} is the P3-radar estimate.

Among the involved rain rates, $R_{std\text{-}V4}$, R_{kR}, and R_{P3} are computed with similar hypothesis concerning the DSD model. The computation relies on the use of constant initial N_0^* for each rain type, which keeps the comparison fully coherent. This is not the case for R_{N0} which implies N_0^*-scaling with point-to-point adjusted N_0^*, in version 4. Therefore, it is useful to evaluate change of the "reference" R_{P3} (to R_{P3}') when N_0^*-scaling is also used in the processing of P3-radar data, i. e. in the calibration process, and the estimation of R from a N_0^*-scaled R-Z relation at X-band (see section 5.1). The reference rain rate decreases slightly: $\langle R_{P3}' \rangle / \langle R_{P3} \rangle \approx 0.87$ for total rain in the [2-4] km height range. The change is not as large as it could be expected because effects of increasing N_0^*, and decreasing Z (as a result of the P3-radar calibration correction that becomes 5.5 dB instead of 6.5 dB), partly compensate for each other in the

normalized R-Z relation at X-band used to get R. Thus, the PR/P3 comparison deteriorates when N_0^*-scaling is coherently used in the two estimates: $\langle R_{N0}\rangle/\langle R_{P3}'\rangle=1.27$ instead of $\langle R_{N0}\rangle/\langle R_{P3}\rangle=1.12$ (cf: Table 5). This points out the need for assessing first the reliability of PR-derived N_0^*-scaling results since any error in adjusted N_0^* may bias the two estimates, R_{N0}, and R_{P3}'. The previous considerations also apply to the comparison of the standard version-5, $R_{std\text{-}V5}$, with R_{P3}, since the former relies on the Kozu's N_0-adjustment (cf: section 2.2) while the latter does not. However, there is no analytical way to check including such N_0-adjustment in the computation of R_{P3}.

5.3 Analysis of TRMM PR/P3-radar comparison results in hurricane Brett

For hurricane Brett, version-5 PR products only were used since version-4 products were not available, as already mentioned. The P3-radar data were processed in the same manner as for Bonnie. The P3-radar calibration correction, derived from (38), leads to increase Z_m by 2.7 dB (instead of 6.5 dB in Bonnie, one-year earlier). Fig. 15 displays horizontal cross-sections of attenuation-corrected Z-fields retrieved from the P3-radar (Fig. 15a) and the PR (Fig. 15b) at 3.2 km height. Both fields are shown at the PR beam resolution, and the P3-radar field is corrected for advection. The comparison domain (90 x 80 km^2), centered on the hurricane eye, is also shown. Fig. 15c shows the rain-type classification derived from the PR (from the 2A-23 algorithm). Brett has a smaller size than Bonnie (see Fig. 10). In the comparison area, however, large regions of convective rain exist, in contrast to Bonnie where stratiform rain prevailed. Hence, rain-type dependent comparisons of Z, or R, could be achieved in Brett.

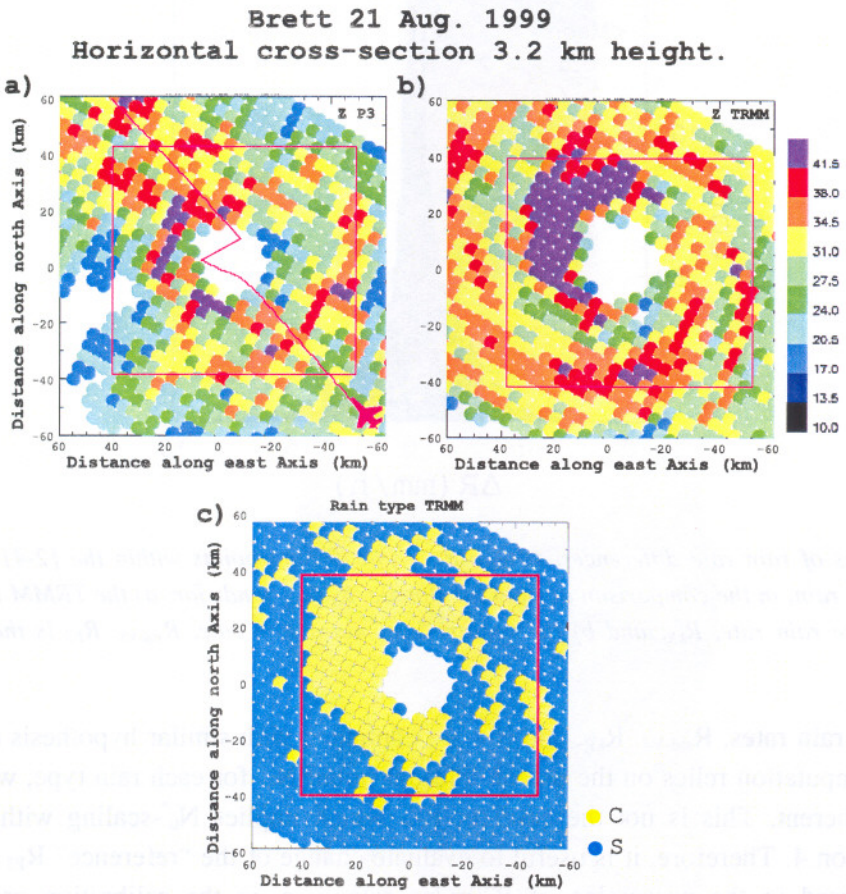

Fig. 15: For hurricane Brett, horizontal cross-section of reflectivity fields at 3.2-km height: a) P3-radar reflectivity, Z_{P3}, corrected for path-attenuation, and radar calibration error; b) TRMM PR attenuation-corrected reflectivity, Z_{TRMM}, from the version-5 2A-25 algorithm. In panel a, the P3–radar field is corrected for advection, and averaged at the PR beam resolution; and the genuine flight-track of the P3-42 aircraft is indicated (two small-radius loops performed within the hurricane eye are not drawn). Panel c displays the rain-type classification index derived from

the PR with S (resp. C) for stratiform (resp. convective) rain. The box delineates the area used for point-to-point comparisons.

Though the two reflectivity patterns have similar shapes, the PR-derived reflectivities are higher than the P3-radar derived ones, especially in convective rain. The mean horizontally-averaged vertical Z-profiles, depending on rain type, are shown in Fig. 16. Results for stratiform rain agree well for the PR and P3-radar estimates. In contrast, for convective rain and total rain, the PR estimate deviates more and more from the P3-radar estimate as altitude decreases below about 4.5 km.

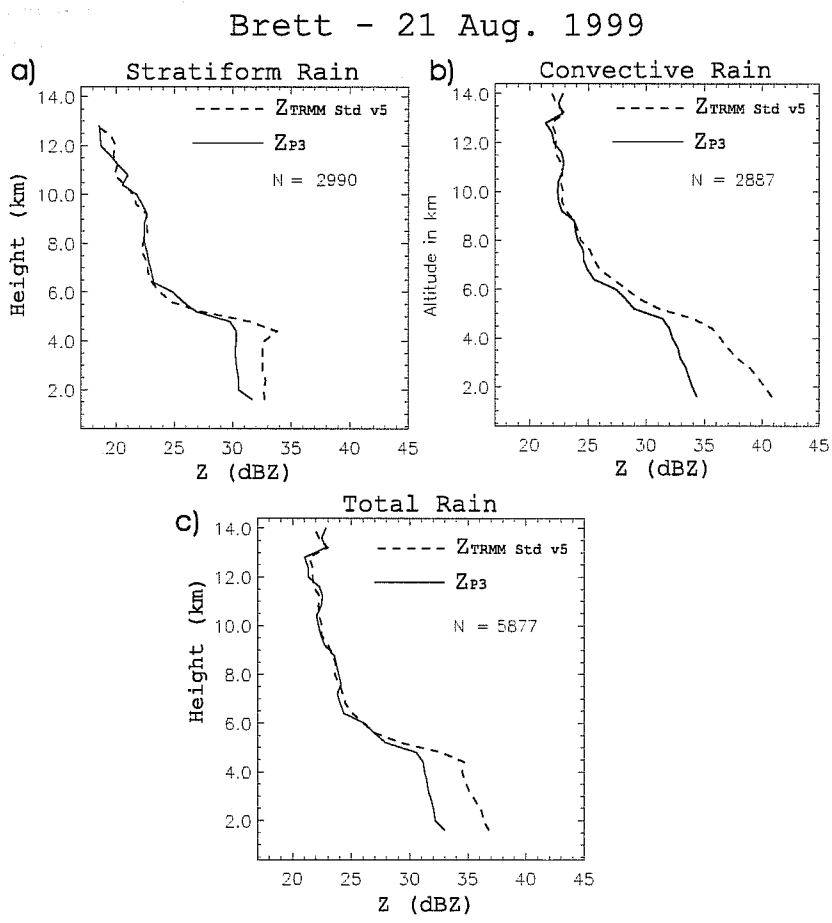

Fig. 16: Mean vertical profiles of horizontally-averaged attenuation-corrected reflectivity factors in the comparison domain for Brett (see Fig. 15). Z_{TRMM} stands for PR version-5 standard estimate. Z_{P3} is the P3-radar estimate. Results are shown for: a) stratiform rain (S), b) convective rain (C), and c) total rain (T).

Bulk results of the rain-type dependent mean difference $\langle \Delta Z \rangle = \langle Z_{TRMM} \rangle - \langle Z_{P3} \rangle$ (and $\langle \Delta R \rangle = \langle R_{TRMM} \rangle - \langle R_{P3} \rangle$), along with the associated standard deviation from the mean, in the [2-4] km altitude range, are listed in Table 6. The ratio of the two mean R estimates $\langle R_{TRMM} \rangle / \langle R_{P3} \rangle$ in the same altitude slab, for each rain type, is also indicated.

Parameter	<Mean>			Std dev.		
	S-Rain	C-rain	T-rain	S-rain	C-rain	T-rain
$(Z_{TRMM}-Z_{P3})$ for V5 (dB)	2.3	5.2	3.7	7.0	8.3	7.8
$(R_{std-V5}-R_{P3})$ (mm/h)	0.7	12.4	6.5	5.0	31.5	24.0
$\langle R_{P3} \rangle$ (mm/h)	4.6	11.8	8.2	-	-	-
$\langle R_{std-V5} \rangle / \langle R_{P3} \rangle$	**1.14**	**1.97**	**1.75**	-	-	-

Table 6: Same as Table 5 but for hurricane Brett, and version-5 results only. Besides, results are given separately for convective (C), stratiform (S), and Total (T) rain.

The observed $<\Delta Z>= 2.3$ dB in stratiform rain agrees fairly well with the theoretical computation $<\Delta Z>_{th}\approx$ 1.1 dB (cf: Appendix 2), though the std dev. is much larger than expected from theory (as in Bonnie case). The residual 1.2-dB offset lies within the margin of errors in the calibration of both radars. For convective and total rain, the observed $<\Delta Z>= 5.2$ dB, and 3.7 dB, respectively, far exceeds the theoretical prediction $<\Delta Z>_{th}\approx$ 1 dB; the residual offsets (exceeding 2 dB) are outside the uncertainty margin of calibration errors. As for the mean rain rate, the PR estimate, in the [2-4] km height range, is 14% above the P3-radar estimate for stratiform rain (4.6 mm h^{-1}), but about twice greater than the P3-radar estimate for convective rain (11.8 mm h^{-1}) or total rain (8.2 mm h^{-1}). Height profiles of the rain-type dependent mean rain rates are shown in Fig. 17. Histogram of rain rate differences, $\Delta R=(R_{TRMM}-R_{P3})$, for stratiform rain that points out the best agreement, is shown in Fig. 18.

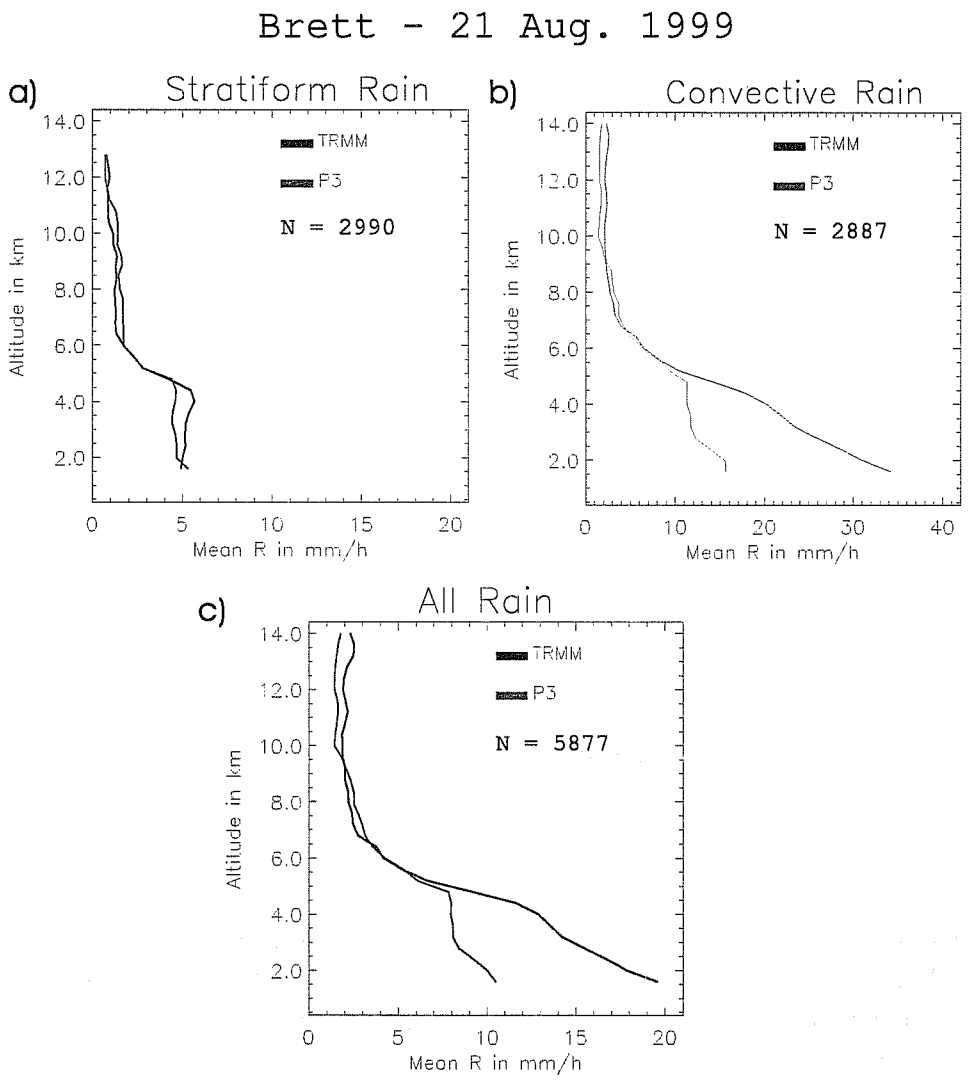

Fig. 17: Mean vertical profiles of horizontally-averaged rain rates in the comparison domain for Brett (see Fig. 15). R_{TRMM} stands for PR version-5 standard estimate. R_{P3} is the P3-radar estimate. Results are shown for: a) stratiform rain (S), b) convective rain (C), and c) total rain (T). Note change in the scale for R in panel b.

A possible explanation to the fact that discrepancies are observed in convective rain (then in total rain), but not in stratiform rain, can be suggested as follows. Strong surface winds over ocean in hurricanes can modify the surface roughness below convective rain, thus corrupt the SR-based total PIA estimate derived from surface echo measurements. In stratiform rain, the corrected Z-profile retrieved from the 2A-25 algorithm is weakly-to-not weighted towards the SR-based solution. Conversely, in convective rain, the highly SR-weighted solution may suffer from the mentioned error in the SR-based PIA estimate. For low off-nadir beam-pointing angles (less than 17 deg for the PR), increase in surface roughness due to surface wind (*Ulaby et al.*, 1982), possibly enhanced by effect of raindrop impact hitting the surface, leads to overestimate the total SR-based PIA, thus to induce an artificial increase in Z (then in R) towards the surface, as observed in PR Z- or R-profile for convective rain (Figs. 16b, and 17b). Such a behavior does not appear in Z- or R-profile for stratiform rain (Fig. 16a, and 17a), but is partly repercuted onto Z- and R-profile for total rain (Fig. 16c and 17c) via the contribution of convective rain. According to (A5) with b≈0.65 in Appendix 1, overestimating the SR-based PIA by 5 dB may increase R by a factor of 2 near the surface, for the "true" SR-case with large PIA. Such characteristics were not depicted in Bonnie because stratiform rain was predominant in the comparison domain. This points out a potential deficiency inherent to the 2A-25 algorithm: the possibly large overestimation of Z (and R) towards the surface in convective rain above ocean in the presence of strong surface winds, as usually encountered in hurricanes.

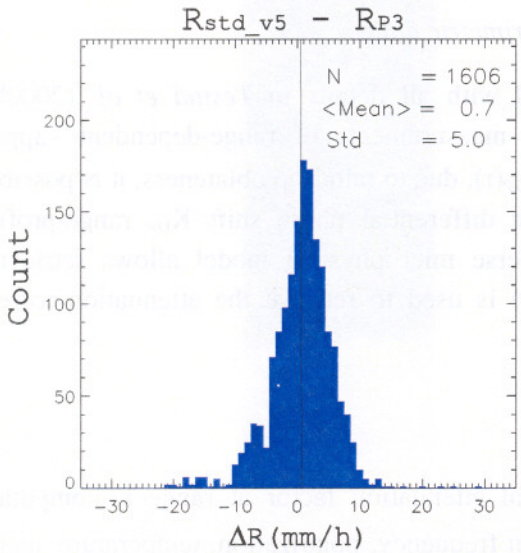

Fig. 18: Histogram of rain rate differences, (R_{TRMM}-R_{P3}), for data points referring to stratiform rain within the [2-4] km height range in the comparison domain for Brett. R_{TRMM} stands for the PR-derived standard version-5 estimate ($R_{std\text{-}V5}$). R_{P3} is the P3-radar estimate.

6. Tests of PR-derived rain parameters using coincident ground-based radar data

Reference rain products used to validate PR products may be also obtained from ground-based radars. Here, we used data of the C-band polarimetric weather radar, located at the GV site of Darwin (Australia), acquired mainly over land on 27 Jan. 1998 during a TRMM overpass (orbit #952). Such comparisons allow us to extend the validation work to other rain systems than hurricanes over ocean; and to apply the new Z-Phi algorithm developed at CETP (*Testud et al.*, 2000b) to exploit polarimetric data. Actually, none of the TRMM standard ground validation (GV) algorithms produces 3-D rain rate field so as to compare it directly with the PR-derived one. Indeed, 3-D reflectivity field, and *surface* rain rate fields only, can be obtained. Meanwhile, 3-D Z- and R-fields obtainable from the Z-Phi algorithm (applied to C-band H/V polarimetric Darwin radar data) can be usefully compared to those derived from the PR. Also, the Z-Phi

algorithm provides estimates of the DSD scaling parameter N_0^*, which can be compared to those derived from the PR.

6.1 Processing of ground-based radar data

6.1.1 Standard GV products

The TRMM GV standard products that are available from the Darwin radar for the present study are both: reflectivity and rain rate estimates, which are generated every round half-hour. The standard GV reflectivity (horizontal polarization) estimates are generated by the TRMM algorithm 2A55, as 3-D Z-fields in cartesian grid with a horizontal resolution of 2 km, and a vertical resolution of 1.5 km. No correction of path-attenuation is performed. Standard GV rain rate estimates are computed as follows (cf : *Kummerow et al.,* 2000). *Surface* rain rate maps with a horizontal resolution of 2 km, are generated by the TRMM algorithm 2A-53, following *Steiner* (1995). The radar-derived rainfall estimates (using $Z= 300R^{1.4}$) are adjusted over locations of «good» raingauges (i.e. having satisfied a quality-control step). A final $Z= AR^{1.4}$ relationship is derived, where $A= 300(R/G)^{1.4}$, R is the total rainfall estimated by the radar, and G is the accumulated rainfall measured by raingauges. The bulk adjustment, applied to one-to-several months of data, is performed separately for convective and stratiform rain, as categorized from the Darwin-radar measurements, which results in convective (resp. stratiform) relationship $A_{conv}R^{1.4}$ (resp. $A_{strat}R^{1.4}$).

6.1.2 The Z-Phi algorithm for polarimetric data

The Z-Phi algorithm is described with all details in *Testud et al.* (2000b). Let us briefly recall its functioning principle. Thanks to measurements of range-dependent «apparent» reflectivity, Z_m, and differential HH/VV phase shift, $\Phi_{DP}(r)$, due to raindrop oblateness, it is possible to define range bounds (r_0 and r_1) within which the specific differential phase shift K_{DP} range-profile is computable. A K_{DP}-k relationship derived from an inverse microphysical model allows retrieving the specific attenuation coefficient profile k(r). Then, k(r) is used to retrieve the attenuation-corrected reflectivity (horizontal polarization), as:

$$Z(r)= Z_m(r)A(r) \tag{39}$$

where $A(r) = 10^{0.2\int_0^r k(s)ds}$ is the total attenuation factor at range r, computable from k(r). The inverse microphysical model, depending on frequency, polarization, temperature, and raindrop oblateness, is also used to relate k(r) to the attenuation-corrected reflectivity Z(r) as:

$$k(r)= aN_0^{*(1-b)}Z(r)^b \tag{40}$$

where N_0^* is the unknown scaling-parameter of the normalized DSD (*Dou et al.*, 1999a, 1999b). Once Z(r) and k(r) are known, N_0^* is obtained from (40), then used into the modeled R-k relationship to estimate the rain rate profile, as:

$$R(r)= pN_0^{*(1-q)}k(r)^q \tag{41}$$

The derived N_0^* is assumed to be constant over each of pre-selected contiguous range intervals $[r_0\text{-}r_1]$ along the path.

Therefore the Z-Phi algorithm gives access to the 3-D *attenuation-corrected* Z-field, the 3-D R-field, and some spatial distribution of the DSD scaling-parameter, N_0^*. In addition, the algorithm allows self-calibration of the radar with an accuracy better than 0.5 dB. The method was successfully validated in

Testud et al. (2000c), using comparisons of retrieved rain accumulation with those measured with a raingauge network in the reach of the radar.

6.1.3 Geometric considerations for comparisons

Before comparing rain estimates derived from the PR and Darwin radar, it is worth moving first on the following two geometrical considerations.

Firstly, the Darwin radar operates volume scannings within a 120-km maximum range. At present, the Z-Phi algorithm is usable for raindrops only. Hence, comparisons involving Z-Phi algorithm (for ranges between 20 and 120 km from the radar) were limited to elevation angles less than 10 deg, in order to process data in rain only (below the bright-band when it is detected).

Secondly, the differences in beam resolutions and viewing angles of the PR and Darwin radar have to be taken into account in the comparisons. This imply that the Darwin-radar "reference" products must be generated at the beam resolution of the PR (in the vicinity of any PR measurement) for useful comparisons. Accordingly, the "reference" Z-field at C-band was obtained by averaging the "high-resolution" Z-data of the Darwin radar at the "low-resolution" of the PR beam using a PR-like beam-weighting function similar to that used to process airborne P3-radar data (see section 5.1). This was applied to GV standard and polarimetric Z-data, as well. The "reference" polarimetric estimates of the DSD scaling-parameter N_0^* (via Z-Phi algorithm), which are further compared with the PR-derived counterpart, were obtained from direct averaging of N_0^*-data at the PR beam-resolution. The "reference" rain rates were generated by using these "reference" Z- and N_0^*-estimates into the normalized relation (at C-band), $R=a\, N_0^{*(1-b)}\, Z^b$, that is properly used in the current Z-Phi algorithm. For standard GV R-estimates, however, the "reference" *surface* rain rate was derived from direct averaging of R-data at the TRMM beam resolution.

The above-mentioned "reference" 3-D products (Z, R ,and N_0^*) from Z-Phi algorithm, are hereafter labelled as $X_{Dar\text{-}P}$ (index P for polarimetric). The standard GV "reference" products (3-D Z, and *surface* rain rate) are hereafter labelled as $X_{Dar\text{-}S}$ (index S for standard).

6.2 Analysis of TRMM PR/Darwin-radar comparison results

The results discussed here deal with a rainy system observed mainly over land in the reach of the Darwin radar (12.25 S, 131.04 E) during a "good" TRMM overpass, which occured near 0537 UT on 27th Jan. 1998. The polarimetric data were acquired during a 10-min time sequence of the Darwin radar near 0540 UT. Standard GV products refer to 0530 UT. The time delay between the Darwin-radar measurements and the TRMM overpass (lasting $\approx$ 1 min) is short enough to allow point-to-point comparisons with PR-derived rain products.

Fig. 19 displays three horizontal cross sections of the mean reflectivity in the [2-4] km altitude range. The first map (top) displays the version-4 2A-25 standard estimate in the PR swath. The second one (bottom left) shows the Darwin-radar standard GV product averaged at the PR beam resolution within the 120-km maximum range from the radar. The third one (bottom right) displays the reflectivity retrieved from Z-Phi algorithm, also averaged at the PR beam resolution. Results point out good qualitative agreement between the three Z-fields. Similar structures are equally recovered from the PR and Darwin radar in commonly observed regions.

TRMM PR / std-V4 2A-25

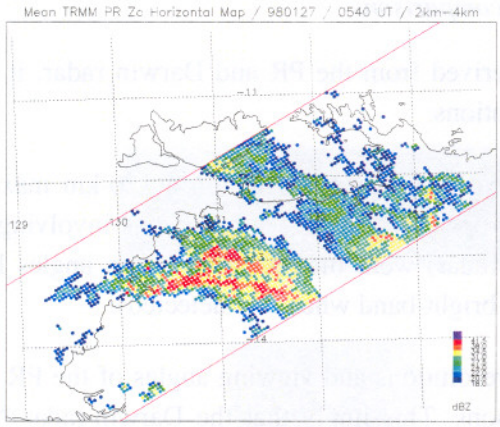

Darwin / GV-standard

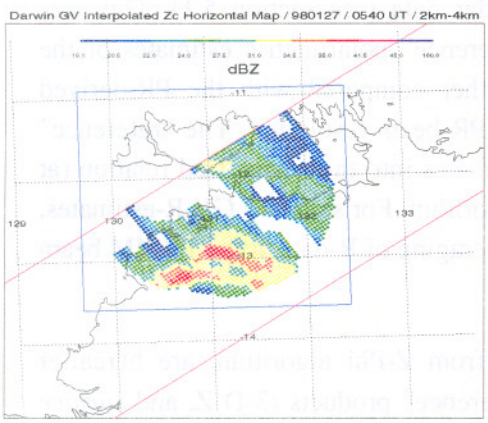

Darwin / Z-Phi

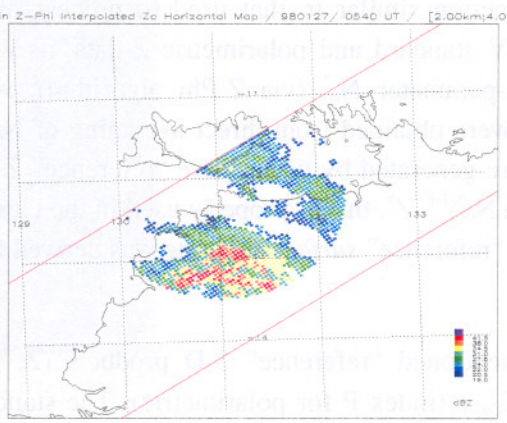

Fig. 19: Horizontal cross-sections of the mean reflectivity between 2- and 4-km altitude, as derived on 27 Jan. 98, from: a) the TRMM PR standard version-4 2A-25, $Z_{std\text{-}V4}$, for orbit #952 (top); b) the Darwin-radar with GV-standard, $Z_{Dar\text{-}S}$ (bottom left); c) the Darwin-radar with Z-Phi algorithm, $Z_{Dar\text{-}P}$ (bottom right). Darwin-radar fields are drawn at the PR beam resolution within the 120-km maximum range from the radar. The PR swath is indicated in all panels.

6.2.1 Results using TRMM GV standard products for the Darwin radar

Results of comparing PR products, and Darwin-radar standard GV products at the PR beam resolution, are summarized in Table 7. Rain rates refer to estimates *close to the surface*. For the GV radar, the *surface* rain rate refers to a constant altitude of 500 m (above surface level). For the PR, however, the so-called *near-surface* rain rate refers, for every path, to the first range gate aloft that is not contaminated by surface clutter; the altitude (above surface level) of the range gate in question increases from 250 m at nadir to about 2 km at swath edges (i. e. for off-nadir beam-pointing angle of 17 deg.). Stratiform (resp. convective) rain, as categorized from the PR, occupies 90% (resp. 10%) of the comparison domain.

Fig. 20 displays rain-type-dependent comparisons of reflectivities, in the [2-4] km altitude range, derived from the PR (version 4 or version 5) and the Darwin-radar ($Z_{Dar\text{-}S}$). The PR-derived rain classification (2A-

23 algorithm) was used to sort results with respect to rain type. According to Table 7, for total rain, the mean difference, $\langle \Delta Z \rangle = \langle Z_{TRMM} \rangle - \langle Z_{Dar\text{-}S} \rangle$, is 0.49 dB with a std dev. of 3.24 dB for the PR version 4; and 1.05 dB with a std dev. of 3.22 dB for the PR version 5. Change in $\langle \Delta Z \rangle$ is mainly due to changing the radar calibration by 0.5 dB in version 5 (cf: section 2.2) with respect to version-4 in the PR-estimate, which provides $\langle Z_{std\text{-}V5} \rangle$ sligthly above $\langle Z_{std\text{-}V4} \rangle$. $\langle \Delta Z \rangle$ is not expected to be zero owing to differences in frequency (C- and K_u-bands) and viewing geometry of both radars. For both PR versions, the observed $\langle \Delta Z \rangle$ for total rain agree rather well with $\langle \Delta Z \rangle_{th} \approx 1$ dB expected from theoretical computation (see Appendix 2). Residual offsets from theory (0.51 dB for the PR version 4, and 0.05 dB for the PR version 5) lie within the uncertainty margin (≈1.5 dB) compatible with calibration errors in both radars (about 1 dB for the PR, and 0.5 dB for the Darwin-radar).

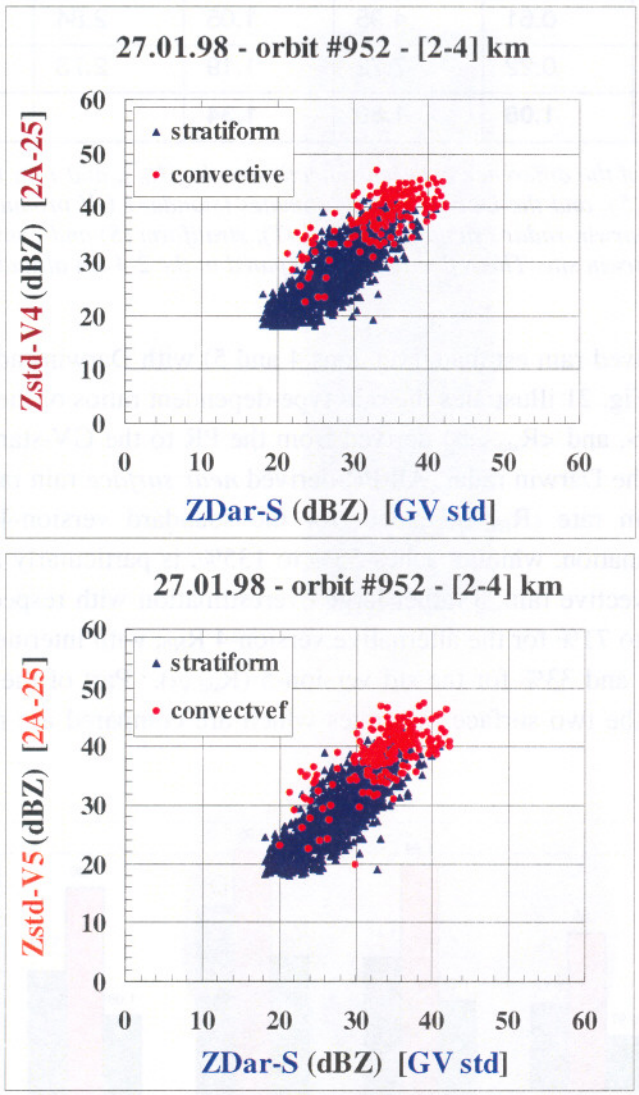

Fig. 20: Comparison of reflectivities retrieved from the TRMM PR and Darwin-radar, for data points within the [2-4] km altitude range, using the GV-standard product (ZDar-S) for Darwin, and version-4 Zstd-V4 (top panel), or version-5 Zstd-V5 (bottom panel) for the PR. Results are shown for stratiform or convective rain, as categorized by the PR.

Parameter	<Mean>			Std dev.		
	C-Rain	S-rain	T-rain	C-rain	S-rain	T-rain
(Z_{std-V4}-Z_{Dar-S}) (dB)	0.08	4.67	0.49	2.90	3.64	3.24
<R_{Dar_S}> (mm/h)	2.76	9.97	3.57	-	-	-
(R_{std-V4} - R_{Dar_S}) (mm/h)	-0.08	5.52	0.55	2.61	9.92	4.49
<R_{std-V4}> / <R_{Dar_S}>	**0.97**	**1.55**	**1.15**	-	-	-
(R_{kR} – R_{Dar-S}) (mm/h)	0.46	9.33	1.39	3.08	12.03	5.57
<R_{kR}> / <R_{Dar-S}>	**1.17**	**1.94**	**1.41**	-	-	-
(R_{N0} - R_{Dar-S}) (mm/h)	1.09	13.40	2.35	3.94	14.73	7.08
<R_{N0}> / <R_{Dar-S}>	**1.42**	**2.35**	**1.71**	-	-	-
(Z_{std-V5}-Z_{Dar-S}) (dB)	0.61	4.95	1.05	2.84	3.76	3.22
(R_{std-V5}-R_{Dar-S}) (mm/h)	0.22	7.72	1.19	2.73	15.37	6.58
<R_{std-V5}> / <R_{Dar-S}>	**1.08**	**1.80**	**1.34**	-	-	-

Table 7: Mean and std dev. of the difference between reflectivities, log(N_0^*), and rain rate estimates, derived from the PR (versions 4 and 5), and the Darwin-radar estimates (standard GV products); and ratio of each PR-derived estimate to the Darwin-radar estimate, for total (T), stratiform (S) and convective (C) rain, in the 27th Jan. 1998 storm over Darwin site. The reflectivity is computed in the 2-4 km altitude range. The rain rate is computed near the surface.

Results of comparing PR-derived rain estimate (versions 4 and 5) with Darwin-radar estimate <R_{Dar-P}> are also summarized in Table 7. Fig. 21 illustrates the rain-type-dependent ratios of the mean *near surface* rain rates (<R_{std-V4}>, <R_{N0}>, <R_{kR}>, and <R_{std-V5}>) derived from the PR to the GV-standard mean *surface* rain rate (<R_{Dar-S}>) derived from the Darwin radar. All PR-derived *near surface* rain rates tend to overestimate the GV-standard *surface* rain rate (R_{Dar-S}), except for the sdandard version-4 in stratiform rain. In convective rain, this overestimation, which reaches 55% to 135%, is particularly large. For total rain that combines stratiform and convective rain, a rather large overestimation with respect to R_{Dar-S} persits: 15% for the std version-4 (R_{std-V4}) to 71% for the alternative version-4 R_{N0}; with intermediate values of 41% for the alternative version-4 R_{kR}, and 33% for the std version-5 (R_{std-V5}). Part of the observed discrepancies may be due to the fact that the two surface rain rates which are compared are not defined in the same manner, as explained above.

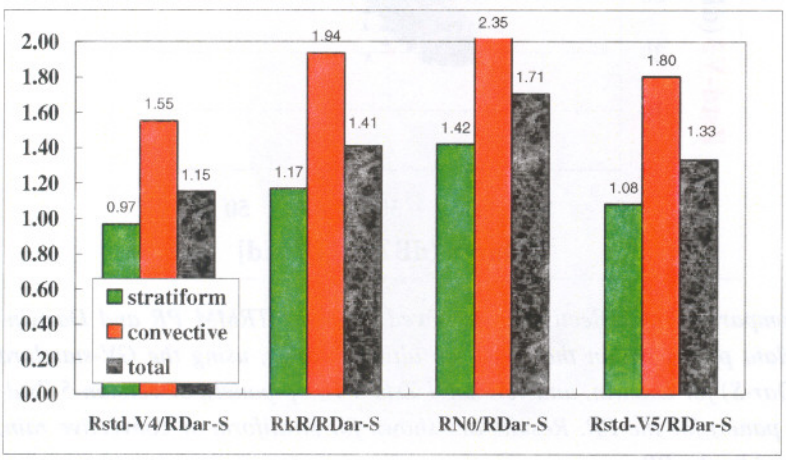

Fig. 21: Ratio of each of the mean near surface rain rates from the PR 2A-25 algorithm (version-4 standard <Rstd-V4>; version-4 alternatives <RkR> and <RN0>; and version-5 standard <Rstd-V5>) to the GV-standard mean surface rain rate (<RDar-S>) from the Darwin-radar. Results are shown for different rain types, as categorized from the PR (cf: Table 7).

6.2.2 Results using Z-Phi polarimetric algorithm products for the Darwin radar

Results of the comparing PR products, and Darwin polarimetric products (Z-Phi algorithm) at the PR beam resolution, are summarized in Table 8. The presentation is the same as in Table 7 (standard products), except that N_0^*-scaling results are added, and rain rates are estimated in the [2-4]-km altitude range in both cases instead of near the surface. In the comparison domain (more restricted than for GV-standard products), stratiform (resp. convective) rain, as categorized from the PR, represents 82% (resp. 18%) of the sample.

Fig. 22 displays rain-type-dependent comparisons of reflectivities, in the [2-4] km altitude range, derived from the PR (versions 4 and 5), and the Darwin-radar ($Z_{Dar\text{-}P}$). The presentation is similar to that of Fig. 20 (GV-standard products) According to Table 8, for total rain, the mean difference, $\langle\Delta Z\rangle = \langle Z_{TRMM}\rangle - \langle Z_{Dar\text{-}P}\rangle$, is 0.21 dB with a std dev. of 4.11 dB for the PR version 4; and 0.84 dB with a std dev. of 4.10dB for the PR version 5. Change in $\langle\Delta Z\rangle$ still results from changing the radar calibration by 0.5 dB in version 5 (cf: section 2.2). Again, it is not expected that $\langle\Delta Z\rangle$ be zero. The observed $\langle\Delta Z\rangle$ are close to the theoretical expectation $\langle\Delta Z\rangle_{th} \approx 1$ dB (see Appendix 2). Like for comparison results involving standard GV reflectivities (cf: section 6.2.1), residual offsets from theory (0.79 dB for version 4, and 0.16 dB for version 5) still stay within the uncertainty margin (≈1.5 dB) due to calibration errors in both radars. Note that the capability of self-calibration capability of the Darwin-radar in Z-Phi algorithm processing adds a calibration correction of about 1 dB with respect to the standard case, which generates a final decrease of $\langle\Delta Z\rangle$ of about 0.3 dB.

Parameter	<Mean>			Std dev.		
	S-Rain	C-rain	T-rain	S-rain	C-rain	T-rain
$(Z_{std\text{-}V4} - Z_{Dar\text{-}P})$ (dB)	-0.12	1.80	0.21	3.70	5.44	4.11
$\langle \log N_0^*{}_{Dar\text{-}P} \rangle$	7.171	7.196	7.175	-	-	-
$(\log N_0^*{}_{V4} - \log N_0^*{}_{Dar\text{-}P})$	-0.101	0.483	0.001	0.714	0.469	0.713
$\langle R_{Dar\text{-}P} \rangle$ (mm/h)	6.78	17.68	8.68	-	-	-
$(R_{std\text{-}V4} - R_{Dar\text{-}P})$ (mm/h)	-2.81	-1.40	-2.08	5.62	14.32	8.00
$\langle R_{std\text{-}V4} \rangle / \langle R_{Dar\text{-}P} \rangle$	**0.58**	**1.08**	**0.76**	-	-	-
$(R_{kR} - R_{Dar\text{-}P})$ (mm/h)	-1.78	6.58	-0.32	5.81	15.24	8.84
$\langle R_{kR} \rangle / \langle R_{Dar\text{-}P} \rangle$	**0.74**	**1.37**	**0.96**	-	-	-
$(R_{N0} - R_{Dar\text{-}P})$ (mm/h)	-0.89	11.25	1.31	6.31	16.79	10.13
$\langle R_{N0} \rangle / \langle R_{Dar\text{-}P} \rangle$	**0.88**	**1.63**	**1.15**	-	-	-
$(Z_{std\text{-}V5} - Z_{Dar\text{-}P})$ (dB)	0.51	2.28	0.84	3.76	5.14	4.10
$(\log N_0^*{}_{std\text{-}V5} - \log N_0^*{}_{Dar\text{-}P})$	-0.302	0.066	-0.235	0.370	0.343	0.391
$(R_{std\text{-}V5} - R_{Dar\text{-}P})$ (mm/h)	-1.96	4.99	-0.69	5.56	17.54	9.39
$\langle R_{std\text{-}V5} \rangle / \langle R_{Dar\text{-}P} \rangle$	**0.71**	**1.28**	**0.92**	-	-	-

Table 8: Mean and std dev. of the difference between reflectivities, $\log(N_0^*)$ with N_0^* in m^{-4}, and rain rate estimates, derived from the PR (versions 4 and 5), and the Darwin-radar estimates (Z-Phi algorithm); and ratio of each PR-derived estimate to the Darwin-radar estimate, for total (T), stratiform (S) and convective (C) rain, in the 27th Jan. 1998 storm over Darwin site. Each parameter is computed in the 2-4 km altitude range. For N_0^*, a difference of 0.3 in log unit corresponds to a ratio of 2 of the involved two quantities.

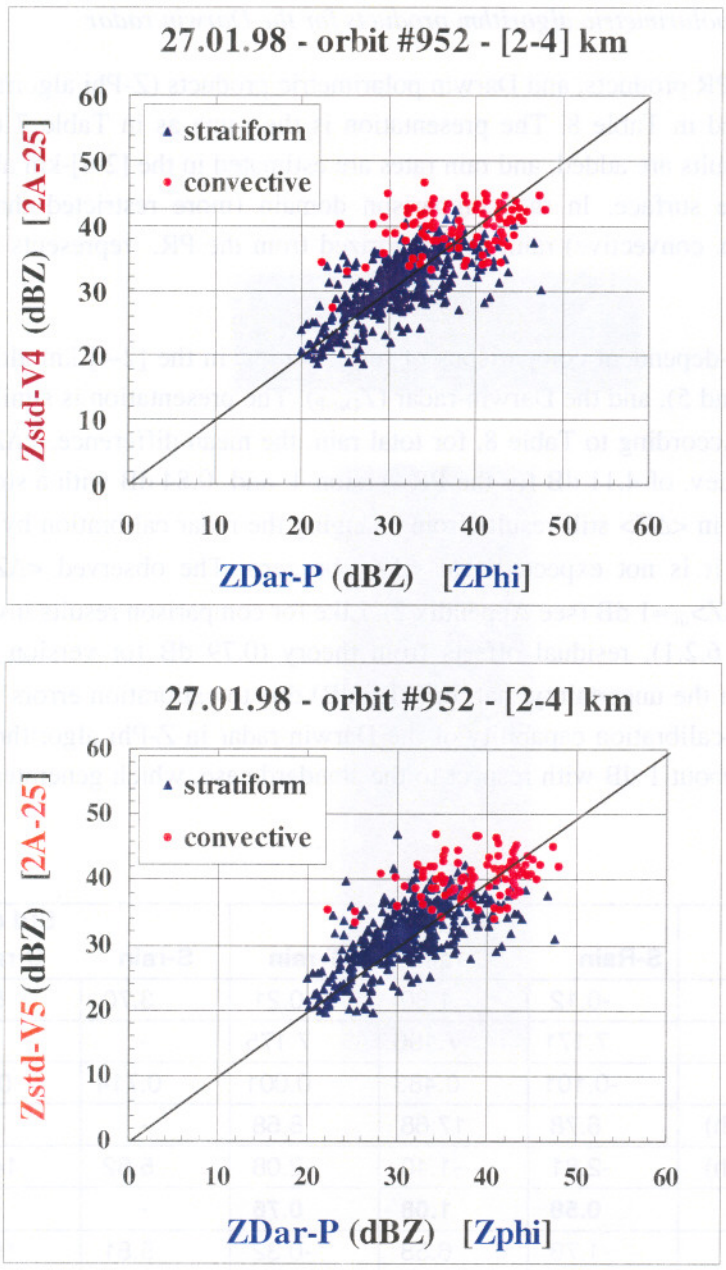

Fig 22: Same as Fig. 20, but for Darwin-radar reflectivity ($Z_{RDar\text{-}P}$) estimated from the Z-Phi polarimetric algorithm instead of GV-standard algorithm. Results are shown for different rain types, as categorized from the PR.

Fig. 23 displays rain-type-dependent comparisons of N_0^*-estimates (in log-unit), in rain, from the PR (version 4 or version 5), and Darwin-radar. For version 4, $\log(N_0^*)$ retrievals lie within a fairly-well confined region (6 to 8 in log-scale) close to the bisectrix, without clear distinction according to rain type. For version 5, $\log(N_0^*)$ retrievals are concentrated in a quite-well confined region close to the bisectrix, and point out a clear splitting according to rain type. This is worthy of note, considering that N_0^* is retrieved by quite different ways from the Darwin-radar ("constant" over range intervals along nearly horizontal paths from Z-Phi algorithm), and from the PR ("constant" over nearly vertical paths from 2A-25 algorithm). According to Table 8, the mean differences in $\log(N_0^*)$ between the PR version-4 and Darwin results are -0.101, 0.483, and -0.001, for stratiform, convective, and total rain, respectively; despite a rather

large std dev. from the mean in each case. For version 5, the mean differences are -0.302, 0.066, and -0.235, for stratiform, convective, and total rain, respectively; they are slightly different from version-4 (except in convective rain), but the std dev. from the mean is significantly reduced in each case, pointing out better agreement with Darwin polarimetric estimates. These results provide reasonable credibility to N_0^*-scaling derived from the PR, especially for version-5 results (though N_0^*-scaling is not used in practice in the PR version-5 standard 2A-25 algorithm).

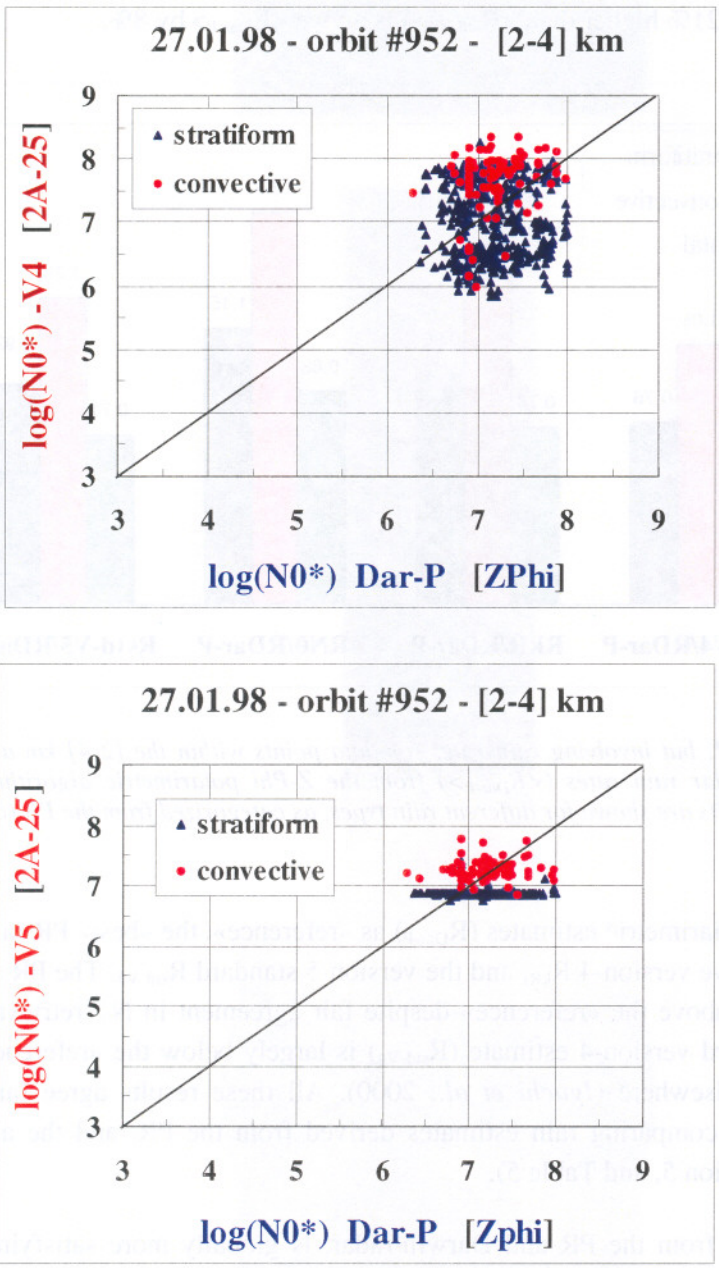

Fig. 23: Comparison of $\log(N_0^*)$ (N_0^* in m^{-4}), in rain, retrieved from the PR version-4 (top panel), or version-5 (bottom panel) 2A-25 algorithm, with those retrieved from the Darwin-radar via the Z-Phi polarimetric algorithm, for data points within the [2-4] km altitude range. Results are shown for different rain types, as categorized from the PR.

Results of comparing PR-derived rain estimate (versions 4 and 5) with the Darwin-radar polarimetric estimate $\langle R_{Dar\text{-}P} \rangle$ are also summarized in Table 8. Fig. 24 illustrates the rain-type-dependent ratio of each mean rain rate ($\langle R_{std\text{-}V4} \rangle$, $\langle R_{N0} \rangle$, $\langle R_{kR} \rangle$, and $\langle R_{std\text{-}V5} \rangle$) derived from the PR, to the Darwin-radar mean rain

rate estimate (<$R_{Dar\text{-}P}$>), in the [2-4] km altitude range. The presentation is similar to that of Fig. 21 (GV-standard products). A sytematic tendency is observed for all TRMM PR rain rates to underestimate (overestimate) the «reference» Darwin rain rate ($R_{Dar\text{-}P}$) in stratiform (resp. convective) rain. For convective rain, the overestimation is much less than with GV-standard products. For total rain, which combines the two rain types, it is observed that: i) the PR version-4 standard estimate <$R_{std\text{-}V4}$> is below <$R_{Dar\text{-}P}$> by 24%; ii) the PR version-4 alternatives <R_{kR}> (26% higher than <$R_{std\text{-}V4}$>), and <R_{N0}> (51% higher than <$R_{std\text{-}V4}$>) is below <$R_{Dar\text{-}P}$> by 4%, and above <$R_{Dar\text{-}P}$> by 15%, respectively; iii) the PR version-5 standard $R_{std\text{-}V5}$ (21% higher than <$R_{std\text{-}V4}$>) is above <$R_{Dar\text{-}P}$> by 8%.

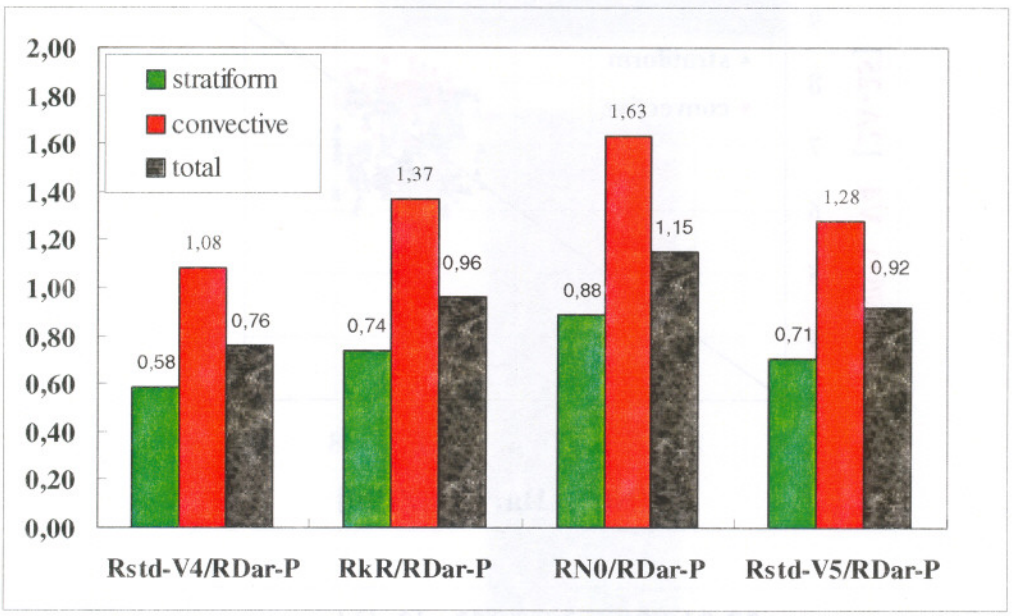

Fig. 24: Same as Fig. 21, but involving rain rates for data points within the [2-4] km altitude range, and « reference » Darwin-radar rain rates (<$R_{Dar\text{-}P}$>) from the Z-Phi polarimetric algorithm instead of GV-standard algorithm. Results are shown for different rain types, as categorized from the PR (cf: Table 8).

Therefore, when taking polarimetric estimates ($R_{Dar\text{-}P}$) as «reference», the «best» PR rain rate estimates, for total rain, are the alternative version-4 R_{kR}, and the version-5 standard $R_{std\text{-}V5}$. The PR alternative version-4 estimate, R_{N0}, is slightly above the «reference» despite fair agreement in N_0^* retrievals from the PR and Darwin-radar. The standard version-4 estimate ($R_{std\text{-}V4}$) is largely below the «reference», which confirms the deficiency reported elsewhere (*Iguchi et al.*, 2000). All these results agree fairly well with those obtained previouly while comparing rain estimates derived from the PR, and the airborne P3-radar, in hurricane Bonnie (see section 5, and Table 5).

Comparison of rain rates from the PR and Darwin-radar, is globally more satisfying with polarimetric estimates (Dar-P) than with GV standard estimates (Dar-S), previously discussed (see section 6.2.1). Considering that PR and Darwin-radar Z-fields agree fairly well whatever the Darwin estimate (GV-standard or polarimetric), it is likely that the observed bulk improvement of rain rate comparison with the polarimetric estimate is a result of N_0^*-adjustment that is performed in Z-Phi algorithm, and ignored in GV standard product. In the studied case, this leads to an underestimation of the rain rate(s) by the GV-standard (with respect to the polarimetric estimate) which likely explains the increased deviations from the PR estimate(s).

7. Conclusions

Testing improvements brought by changes in the standard versions of TRMM algorithms, and/or suggesting modifications aimed at improving these algorithms, is a sound work for TRMM experimenters. Potential improvements in rain rate estimates from the TRMM PR standard version-4 2A-25 profiling algorithm were explored using different ways to adjust the involved rain relations. Also, changes from the previous standard version-4 ($R_{std\text{-}V4}$) to the presently-operating standard version-5 ($R_{std\text{-}V5}$), were analyzed. Two alternatives to the standard version-4 were derived. They rely on using either constant R-k relation (R_{kR}), or N_0^*-scaled relations (R_{N0}) exploiting the concept of normalized Γ-shaped DSD, instead of constant R-Z relation as in $R_{std\text{-}V4}$. The computational parameters can be easily derived from the standard 2A-25 output file without need for reprocessing the algorithm. Analysis of errors in N_0^*-scaling and R-estimates was conducted. The alternatives R-estimates appear less sensitive to unknown errors in radar calibration, or initial relations, than the standard. Conceptually, R_{N0} is the most attractive but its reliability is questionable owing to inherent effects of errors in N_0^*-scaling. If N_0^*-scaling is not used, R_{kR} is expected to be more reliable than the standard. Examination of such alternatives is useful to assess effects of various error sources and determine limits on accuracy expected from a single-frequency radar such as TRMM PR.

The above-mentioned approaches were analyzed from PR observations in hurricane Bonnie, and their mean features were pointed out from a PR data set (13 orbits) over ocean and land. The version-4 2A-25 yields adjusted N_0^* systematically larger than the initial values. The alternative R-estimates, higher than $R_{std\text{-}V4}$ (by about 25% for R_{kR}, and 50% for R_{N0}) for total rain, may correct for some reported underestimation of the rain rate by the standard. The new standard version-5 points out an improved functioning of the algortithm with respect to version 4: the correction factor has much less spread and its mean is closer to unity, the need for large N_0^*-adjustment disappears, and $R_{std\text{-}V5}$ increases the total rain rate estimation by about 30%. No differences were obtained for observations over ocean or land, which might result from the fact that land cases refer to observations made in the vicinity of Darwin site (Australia) near ocean, only.

For better testing TRMM PR products, 3-D PR-derived Z- and R-fields were first compared with «reference» fields derived from airborne X-band dual-beam radar, on board NOAA/P3-42 aircraft, in hurricanes Bonnie and Brett, for good cases of TRMM overpass over ocean. Special attention was brought to respect proper conditions for the comparisons. This involved, in particular, a small time lag between both data sets, rain-type dependent estimations from P3-radar, and averaging of the P3-radar data at the PR beam resolution. Results deteriorate significantly when such conditions are not fulfilled. Version-4 (for Bonnie) and version-5 (for Bonnie and Brett) PR products were used in the comparisons.

For Bonnie, dominated by stratiform rain in the comparison domain, the observed mean difference, $\langle \Delta Z \rangle = \langle Z_{TRMM} - Z_{P3} \rangle$, in the [2-4] km altitude range, is weak (-0.7 dB for version 4, and -0.2 dB for version 5), and agrees with the value (≈1 dB) expected from theory (K_u-band verssus X-band). The residual offsets are compatible with the uncertainty margin due to errors in the calibration of both radars. Comparison of mean R-profiles for total (mainly stratiform) rain shows that the version-5 standard ($R_{sdt\text{-}V5}$), and the version-4 alternatives (R_{kR} and R_{N0}), are higher than the standard version-4 ($R_{std\text{-}V4}$) by 15%, 19%, and 39%, respectively. R_{kR} and $R_{std\text{-}V5}$ agree with the P3-radar «reference» R_{P3} within a 5%- and 8%-margin, respectively; while $R_{std\text{-}V4}$ (resp. R_{N0}) is smaller (resp. higher) than R_{P3} by 20% (resp. 11%). Therefore, the version-4 alternative, R_{kR}, or the version-5 standard, $R_{std\text{-}V5}$, corrects rather well for the identified deficiency of the version-4 standard estimate.

For Brett case, comparisons could be made for convective and stratiform rain, separately. In stratiform rain, like in Bonnie results, the observed mean difference $<\Delta Z>=2.3$ dB, in the [2-4] km altitude range is close to that ($\approx$1.1 dB) expected from theory. Again, residual offsets lie within the margin of errors in the calibration of both radars; besides, $R_{tsd\text{-}V5}$ is higher than R_{P3} by 14%. This is not the case for convective or total rain: the mean differences $<\Delta Z>=$ 5.2 dB (convective rain), and 3.7 dB (total rain), leave residual offsets largely outside the uncertainty margin in the radar calibrations; and $<R_{std\text{-}V5}>$ exceeds $<R_{P3}>$ by a factor of about 2 in both cases. A possible explanation of such discrepancies is a corruption of the SR-like solution of the algorithm in convective rain, via overestimated SR-based total PIA due to changes in surface roughness in the presence of strong surface winds. This points out an inherent limit of the 2A-25 algorithm in such conditions.

Also, TRMM PR-derived Z- and R-fields (versions 4 and 5) were tested by comparison with «reference» fields derived from the polarimetric C-band weather radar of Darwin (Australia) at TRMM GV site, for a good case of TRMM overpass in a rainy system (27 Jan. 1998) located mainly over land. Small time lag between both data sets, as well as averaging of the Darwin-radar data at the PR beam resolution, allowed us to perform significant point-to-point comparisons.

The Darwin-radar products included GV-standard estimates from the 2A-53 and 2A-55 TRMM GV algorithms (Dar-S products), and hopefully improved estimates from the Z-Phi polarimetric algorithm (Dar-P products) that provides also estimates of N_0^*. The mean differences in reflectivity $<\Delta Z>=<Z_{TRMM}-Z_{Dar}>$, in the [2-4] km altitude range, for the Dar-S or Dar-P estimates, are close to theoretical prediction (K_u- versus C-band). The residual offsets lie within the uncertainty margin due to errors in the calibration of both radars. Adjusted N_0^* retrieved from the PR 2A-25 algorithm and Z-Phi algorithmn (Dar-P product) are in fair agreement for the PR version 4, and in good agreement for the PR version 5. For total rain, the PR mean *near-surface* rain rate is largely above the mean GV-standard *surface* rain rate (Dar-S product), especially in convective rain. Better agreement is found between the PR mean rain rates, in the [2-4] km altitude range, and the mean polarimetric estimate (Dar-P product). For total rain, the «best» PR-estimates are the version-4 alternative R_{kR} (4% below $R_{Dar\text{-}P}$), and the version-5 standard $R_{std\text{-}V5}$ (8% below $R_{Dar\text{-}P}$). The version-4 alternative R_{N0} overestimates $R_{Dar\text{-}P}$ (by 15%), and the version-4 standard $R_{std\text{-}V4}$ underestimates $R_{Dar\text{-}P}$ (by 24%). We tentatively interpreted the improvement in PR/Darwin-radar rain rate comparison that is observed when using polarimetric instead of GV-standard, as resulting from the use of N_0^*-scaled R(Z) relation in the Z-Phi polarimetric algorithm.

The above-mentioned results must be considered as preliminary owing to the small number of processed cases. More cases shoud be studied to reach definite conclusions. However, in the framework of Euro TRMM, the present study, as well as other ones by various teams around the world, point out reasonable reliability of the TRMM PR 2A-25 algoritm, despite some identified inherent deficiencies. Moreover, aside possible improvements that we proposed for the (previously-operating) standard version 4, the bulk improvements brought by the new (presently-operating) standard version-5 are quite encouraging. The study also demonstrated the high interest of using «reference» rain products from airborne radar and/or ground-based *polarimetric* radar to validate PR-derived rain products, provided that proper conditions (such as a short time delay between data sets, and averaging of reference products at PR beam resolution) be fulfilled in the comparisons.

Appendix 1: Impact of an error in the SR-based PIA on rain rate estimates

If the surface based-PIA factor $A_s(r_s)$ (hereafter noted A_t) measured from the surface echo attenuation is error free, the «true» rain estimate, R_t, is given by (22) where $\varepsilon \equiv \varepsilon_0$ in the PIA factor at range r, $A(r,\varepsilon)$, given by (20). The ratio of each rain estimate ($R_{std\text{-}V4}$, R_{kR}, or R_{N0}) to R_t was obtained by comparing (22) to (27), (28), or (29), providing (34a,b,c). In the presence of an error δA_t, the SR-based PIA becomes $A_t \delta A_t$, and ε_0 from (6) becomes ε_0' given by:

$$\varepsilon_0' = [1 - A_t^{\beta}\, \delta A_t]\, \gamma^{-1} S(0,r_S)^{-1} \tag{A1}$$

Also, R_t in (22) becomes R_t', involving $A(r,\varepsilon_0')$ instead of $A(r,\varepsilon_0)$. Therefore, using the proper expressions for R_t', and R_t, from (22) yields

$$R_t/R_t' = A(r,\varepsilon_0')^b A(r,\varepsilon_0)^{-b} \tag{A2}$$

Expliciting $A(r,\varepsilon_0)$ and $A(r,\varepsilon_0')$ from (20), using the chain rule relation $S(0,r)=[S(0,r_s)-S(r,r_s)]$, and expliciting $S(0,r_s)$ versus A_t from (6), yields:

$$R_t = \{A_t^{1/\beta} + \gamma\varepsilon_0 S(r,r_s)\}^d \{A_t^{1/\beta}\delta A_t^{1/\beta} + \gamma\varepsilon_0' S(r,r_s)\}^{-d} R_t' \tag{A3}$$

Replacing R_t by (A3) in (34a,b,c) points out the impact of an error δA_t on the rain rate estimates, in addition to errors δC and δN_0^*. Thus, (34a,b,c) referring now to R_t' become:

$$R_{std\text{-}V4} = \delta C^b\, \delta N_0^{*(b-1)}\, E(\delta A_t)\, R_t' \tag{A4a}$$

$$R_{N0} = \delta C^{(b-\beta)/(1-\beta)}\, E(\delta A_t)\, R_t' \tag{A4b}$$

$$R_{kR} = \delta N_0^{*(d-1)}\, E(\delta A_t)\, R_t' \tag{A4c}$$

with $$E(\delta A_t) = [A_t^{\beta}\, \delta A_t^{\beta} + \gamma\varepsilon_0' S(r,r_S)]^d\, [A_t^{\beta} + \gamma\varepsilon_0 S(r,r_S)]^{-d} \tag{A5}$$

It may be verified that E decreases when the PIA and/or the distance $(r_s\text{-}r)$ to the surface increases. Near the surface ($r \approx r_S$), and for large PIA (i. e. $A_t << 1$), $E \approx \delta A_t^b$.

Appendix 2: A data-based model simulating expected differences in Z at X-band (or C-band) and K_u-bands

The observed distribution of differences in Z-fields between the airborne P3-radar (X-band), or the Darwin radar (C-band), and the PR (K_u-band) may result from effects of sampling geometries; effects of DSD and phase variability at the two different frequencies and/or polarizations; errors in the calibration of each radar; and statistical uncertainties in Z measurements. The following model simulates effects of sampling geometry, difference in frequency and polarization, and variability in the DSD, while assuming no error in the radar calibrations.

Let us first consider the case of P3-radar. The model starts from the "reference" R-field derived from the P3-radar over a selected 3-D domain, associated to Z_X-field (at X-band), at the TRMM PR beam resolution, from which it is computed via rain-type dependent R-Z_X relationships. The R-Z_X relations rely on normalized Γ-shaped DSD model fitting to the airborne P3-radar measurement conditions, and tuned with proper rain-type dependent N_0^* for each data point. The reference R-field is used, as well, to generate the expected Z_{Ku}-field (at K_u-band), via relevant normalized Z_{Ku}-R relations fitting, this time, to the TRMM PR measurement conditions. Apart from differences in frequencies, the conditions to be fulfilled when simulating the airborne and the spaceborne radar measurements, are the nearly horizontal (resp. vertical) viewing, and the vertical (resp. horizontal) polarization, for the P3-radar (resp. PR). Thus, the expected distribution of $(Z_{Ku}\text{-}Z_X)$ over the selected 3-D domain, can be easily computed. That gives the

"expected" mean, $<\Delta Z>_{th} = <Z_{Ku}-Z_X>$, and std dev., $\sigma_{Z,th}$, to be compared to the "measured" ones. This data-based model applied to data points in the rain region ([2-4] km height range) of the "comparison domain" provides: $<\Delta Z>_{th} \approx +1$ dB, with $\sigma_{Z,th} \approx 0.2$ dB, for total rain in hurricane Bonnie; and $<\Delta Z>_{th} \approx +1$ dB (convective rain) to 1.1 dB (stratiform rain), with $\sigma_{Z,th} \approx 0.2$ dB, in hurricane Brett.

The same approch has been used to get the expected distribution of differences in reflectivities, $(Z_{Ku}-Z_C)$, between the PR (K_U-band) and the Darwin-radar (C-band). The normalized R-Z_C relation is selected according to proper conditions of Darwin measurements (C-band, nearly horizontal viewing of oblate raindrops, and horizontal polarization). The data-based model applied to the involved "reference" R-field of the Darwin-radar in the rain region ([2-4] km height range) yields: $<\Delta Z>_{th} \approx +1$ dB (convective rain) to 1.1 dB (stratiform or total rain), with $\sigma_{Z,th} \approx 0.2$ dB.

References

*References quoted with * deal with works developed in the framework, or in close relation with the EuroTRMM study.*

Amayenc, P., M. Marzoug, and J. Testud, 1993: Analysis of cross-beam resolution effects in rainfall profile retrieval from a spaceborne radar, *I.E.E.E. Trans. Geosci. Remote Sens.*, **31**, 417-425.

CAMEX-3, cited 1998: Camex-3 Web site homepage [Available on-line from http//ghrc.msfc .nasa.gov/camex3/].

*Dou, X., J. Testud, P. Amayenc, and R. Black, 1999a: The parameterization of rain for a weather radar, *C. R. Acad. Sciences, Earth and Planetary Sciences, Paris*, **328**, 577-582.

*Dou, X., J. Testud, P. Amayenc, and R. Black, 1999b: The concept of "normalized" gamma distribution to describe raindrop spectra, and its use to parameterize rain relations. *Preprints, 29th Intern. Conf. on Radar Meteorology*, Montreal, Canada, Amer. Meteor. Soc., 625-628.

Durden, S. L., E. Im, K. Li, W. Ricketts, A. Tannier, and W. Wilson, 1994: ARMAR: An Airborne Rain-Mapping Radar, *J. Atmos. Oceanic Technol.*, **11**, 727-947.

Durden, S. L., and Z. S. Haddad, 1998: Comparison of radar rainfall retrieval algorithms in convective rain during TOGA-COARE, *J. Atmos. Oceanic Technol.*, **15**, 1091-1096.

*Ferreira, F., and P. Amayenc, 1999): Impact of adjusting rain relations on rain profiling estimates from the TRMM precipitation radar, Proc. 29th Conference on Radar Meteorology, Montreal, Canada, AMS, pp.643-646.

*Ferreira, F., P. Amayenc, S. Oury, and J. Testud, 2001: Study and tests of improved rain estimates from the TRMM precipitation radar, *J. Appl. Meteor.*, **40**, 1979-1899.

Foote , G. B., and P. S. du Toit, 1969: Terminal velocity of raindrops aloft, *J. Appl. Meteor.*, **8**, 249-253.

Hitschfeld, W., and J. Bordan, 1954: Errors inherent in the radar measurement of rainfall at attenuating wavelengths, *J. Meteorol.*, **11**, 58-67.

Iguchi, T., T. Kozu, R. Meneghini, J. Awaka, and K. Okamoto, 2000: Rain profiling algorithm for the TRMM precipitation radar, *J. Appl. Meteor.* (TRMM special issue), **39**, 2038-2052.

Iguchi, T., and R. Meneghini, 1994: Intercomparison of single-frequency methods for retrieving a vertical rain profile from airborne or spaceborne radar data, *J. Atmos. Oceanic Technol.*, **11**, 1507-1516.

Kozu, T., T. Iguchi, K. Shimizu, and N. Kashiwagi, 1999: Estimation of raindrop size distribution parameters using statistical relations between multi-parameter rainfall remote sensing data. *Preprints, 29th Intern. Conf. on Radar Meteorology*, Montreal, Canada, Amer. Meteor. Soc., 689-692.

Kozu, T., and T. Iguchi, 1999: Nonuniform beam filling correction for spaceborne rain radar rainfall measurement: Implication from TOGA-COARE radar data analysis, *J. Atmos. Oceanic Technol.*, **18**, 1722-1735.

Kummerow, C., J. Simpson, O. Thiele, W. Barnes, A. T. C. Chang, E. Stoker, R. F. Adler, A. Hou, R. Kakar, F. Wentz, P. Ashcroft, T. Kozu, Y. Yong, K. Okamoto, T. Iguchi, H. Kuroiwa, E. Im, Z. Haddad, G. Huffman, T. Krishnamurti, B. Ferrier, W. S. Olson, E. Zipser, E. A. Smith, T. T. Wilheit, G. North, and N. Nakamura (2000): The status of the Tropical Rainfall Measuring Mission (TRMM) after 2 years in orbit, *J. Appl. Meteor.* (TRMM special issue), **39**, 1965-1982.

Marécal, M., T. Tani, P. Amayenc, K. Klapisz, E. Obligis, and N. Viltard, 1997: Rain relations inferred from microphysical data in TOGA-COARE and their use to test a rain profiling method from radar measurements at K_u-band, *J. Appl. Meteor.*, **36**, 1629-1646.

Marshall, J. S., and W. M. K. Palmer, 1948: The distribution of raindrops with size, *J. Meteorol.*, **5**, 165-166.

Marzoug, M., and P. Amayenc,1994: A class of single- and dual-frequency algorithms for rain rate profiling from a spaceborne radar. Part I : Principle and tests from numerical simulations, *J. Atmos. Oceanic Technol.*, **11**, 1480-1506.

Meneghini, R., J. Eckerman, and D. Atlas, 1983: Determination of rain rate from a spaceborne radar using measurement of total attenuation, I.E.E.E. Trans. Geosci. Remote Sens., **21**, 38-43.

Meneghini, R., and Nakamura K., 1990: Range profiling of the rain rate by an airborne weather radar, *Remote Sens. Environ.*, **31**, 193, 200.

Meneghini, R., and D. Atlas, 1986: Simultaneous ocean cross section and rainfall measurements from space with nadir-looking radar, J. Atmos. Oceanic Technol., **3**, 400-413.

Meneghini, R., T. Iguchi, T. Kozu, L. LiaoK. Okamoto, J. A. Jones, and J. Kiatkowski, 2000: Use of the surface reference technique for path atrtenuation estimates for the TRMM radar, *J. Appl. Meteor.*, **39**, 2053-2070.

Oury, S., J. Testud, V. Marécal (1998): Estimate of precipitation from the dual beam airborne radars in TOGA-COARE. Part 1: The K-Z relationships derived from the Stereo- and Quad-beam analysis. *J. Appl. Meteor.*, **38**, 156-174.

Oury, S., X. Dou, and J. Testud (2000): Estimate of precipitation from the dual beam airborne radars in TOGA-COARE. Part 2: Precipitation efficiency in the 9th February 1993 MCS, *J. Appl. Meteorol.*, **40**, in press.

Steiner, M., R.A. Houze Jr., and S. E. Yuter (1995): Climatological characterization of three-dimensional storm structure from operational radar and rain gauge data, *J. Appl. Meter.*, **34**, 1978-2007.

Tani, T., and P. Amayenc, 1998: Comparison of rain profiling methods from ARMAR data in TOGA-COARE with a view to a possible use with the TRMM radar, *J. Appl. Meteor.*, **37**, 1600-1618.

*Testud, J., S. Oury, X. Dou, P. Amayenc, and R. Black, 2001: The concept of normalized distribution to describe raindrop spectra: a tool for cloud physics and cloud remote sensing, *J. Appl. Meteor.*, **16**, 1118-1140.

*Testud, J., E. Le Bouar, E. Obligis, and M. Ali-Mehenni, 2000b : The rain profiling algorithm applied to polarimetric weather radar, *J. Atmos. Oceanic Technol.*, **17**, 332-356.

*Le Bouar, E., J. Testud, and T. D. Keenan, 2000c: Validation of the rain profiling algorithm «ZPhi» from the C-band polarimetric weather radar in Darwin, *J. Atmos. Oceanic Technol.*, revised (Nov. 2000).

Ulaby, F. T., R. K. Moore, and A. K. Fung, 1982 : Microwave Remote Sensing, Vol. 2, Addison-Wesley, 1064 pp.

Ulbrich C. W., 1983 : Natural variations in the analytical form of the raindrop size distribution, *J. Climate Appl. Meteor.*, **22**, 1204-1215.

Webster, P. J., and R. Lukas, 1992: TOGA-COARE : The coupled Ocean-Atmosphere Response Experiment, *Bull. Amer. Meteor. Soc.*, **73**, 1377-1416.

Acknowledgements

The Euro TRMM program, funded by European Commission and European Space Agency, involves a consortium of scientists from Centre d'étude des Environnements Terrestre et Planétaires (France), European Center for Medium range Weather Forecast (UK), German Aerospace Research Establishment (Germany), Instituto di Fisica dell'Atmosfera (Italy), Max Planck Institute for Meteorology (Germany), Rutherford Appleton Laboratory (UK), University of Essex (UK), Université Catholique de Louvain (Belgium), and University of Munich (Germany). We wish to thank Dr. T. Iguchi (CRL, Tokyo, Japan) for providing us the code of updated versions of the 2A-25 algorithm; Dr. J. Kwiatkowski (NASA/GSFC/ TSDIS, Greenbelt, USA) for providing us some TRMM PR version-5 data reprocessed before the scheduled date; Dr. F. Marks (NOAA/HRD, Miami, USA) for providing us airborne radar data in hurricanes Bonnie and Brett; and Dr. T. D. Keenan (BMRC, Melbourne, Australia) for providing us data from the Darwin polarimetric radar. We greatly appreciated fruitful discussions with Dr. N. Viltard (CETP, Velizy, France).